Title. Chronic Gq activation of ventral hippocampal neurons and astrocytes differentially affects memory and behavior.

Authors. Rebecca L. Suthard[1,4], Alexandra L. Jellinger[4], Monika Shpokayte[1,4], Michelle Surets[2], Angela Y. Pyo[4], Michelle D. Buzharsky[2], Ryan A. Senne[1,4], Heloise LeBlanc[1,4], Steve Ramirez[3,4]*

Affiliations.

[1]Graduate Program for Neuroscience, Boston University, Boston, MA, 02215

[2]Undergraduate Program in Neuroscience, Boston University, Boston, MA, 02215

[3]Department of Biomedical Engineering, Boston University, Boston, MA, 02215

[4]Department of Psychological and Brain Sciences; The Center for Systems Neuroscience; Neurophotonics Center, and Photonics Center, Boston University, Boston, MA, 02215

*Corresponding Author; dvsteve@bu.edu

Abstract.

Network dysfunction has been implicated in numerous diseases and psychiatric disorders, and the hippocampus serves as a common origin for these abnormalities. In this study, we tested the hypothesis that chronic induction of local changes in neurons and astrocytes is sufficient to induce impairments in cognition and behavior. We chronically activated the hM3D(Gq) pathway in CaMKII+ neurons or GFAP+ astrocytes within the ventral hippocampus across 3, 6 and 9 months. We observed that CaMKII-hM3Dq activation impaired fear acquisition, decreased anxiety and social interaction, and modified spatial odor memory and novel environment exploration, while GFAP-hM3Dq activation impaired fear acquisition and enhanced recall. CaMKII-hM3Dq activation modified the number of microglia, while GFAP-hM3Dq activation impacted microglial morphological characteristics, but neither affected astrocytes. Manipulation of both cell types increased the presence of phosphorylated tau at the earliest time point. Overall, our study provides evidence for how each of these cell types are uniquely engaged in disorders that have characteristic network dysfunction while adding a more direct role for glia in modulating behavior.

Main Points.

- Behaviorally, neuronal Gq activation modified fear, anxiety, social and exploration behaviors, while astrocytic Gq activation induced changes in fear acquisition and recall.
- Cellularly, CaMKII-Gq activation modified microglial number, while GFAP-Gq activation affected microglial morphology. Neither cell manipulation affected astrocytic number or morphology.
- pTau is increased in vHPC at the 3 month time point for both neuronal and astrocytic Gq activation.

1) Introduction.

Cellular disturbances in the inhibitory and excitatory balance of brain circuits have been implicated in various neurodegenerative disorders such as Alzheimer's Disease (AD), Multiple Sclerosis (MS) and Parkinson's Disease (PD) (Lauterborn et al. 2021; Bi et al. 2020; Vico Varela et al. 2019; Lerdkrai et al. 2018; Campanelli et al. 2022; Ellvardt et al. 2018). Additionally, these imbalances, such as neuronal hyperactivity or hypoactivity, have been demonstrated to be core features of psychiatric disorders, including Post-Traumatic Stress Disorder (PTSD), Schizophrenia, and Major Depressive Disorder (MDD) (Badura-Brack et al. 2018; Fang et al. 2018; Clancy et al. 2017; Heckers & Konradi et al. 2014; Vadodaria et al. 2019; Helm et al. 2018). Interestingly, psychiatric disorders are often comorbid with neurodegenerative diseases, especially in the case of AD and MDD (Martin-Sanchez et al. 2021). Along similar lines, psychiatric disorders such as MDD and PTSD significantly elevate the risk of developing neurodegenerative diseases such as AD (Flatt et al. 2018; Ownby et al, 2006; Byers & Yaffe, 2011). Thus, imbalances in circuit-level activity provide a putative shared mechanism underlying different brain disorders of the brain and may serve as a therapeutic target.

Recently, many studies have investigated the role of direct brain modulation for the treatment and prevention of disease (Johnson et al., 2013; Gauthier et al. 2022), though the identity of the perturbed cells remains relatively unknown. For instance, stimulation of brain cells via transmagnetic stimulation (TMS), which is an approved therapy for treatment-resistant MDD, has promising therapeutic value when applied to AD, PD, stroke, schizophrenia, and MS (Weiler et al. 2020; Brys et al. 2016; van Lieshout et al. 2020; Cole et al. 2015; Nasios et al. 2018). However, understanding how to restore brain patterns through a cell-type specific and targeted manner remains elusive, especially when used for the treatment of brain diseases. Hyperactivity is a hallmark of many disorders and often occurs in areas of the brain involved in learning and memory. For instance, the hippocampus (HPC) is a deep brain structure crucially involved in learning and memory, and its connecting sub-regions are crucial for the formation and retrieval of episodic memories in particular (Eichenbaum, Otto & Cohen, 1992; Moser & Moser, 1998; Burgess, Maguire & O'Keefe, 2002; Eichenbaum & Fortin, 2003). Various clinical and preclinical studies have shown that in early disease states of AD, the HPC becomes hyperactive and, therefore, is a prime location for network dysfunction and disconnection from other brain regions (Palop et al. 2007; Busche et al. 2008; Busche et al. 2012; Palop & Mucke, 2016; Klink et al 2021; Anastacio, Matosi, & Ooi, 2022; Kuchibhotla et. al., 2009). One of the major subregions of the HPC that is directly affected in such diseases is the ventral axis, especially ventral CA1 (vCA1; Maruszak & Thuret, 2014). Notably, the ventral HPC (vHPC) has direct connectivity to many downstream regions such as the basolateral amygdala (BLA), nucleus accumbens (NAc), medial prefrontal cortex (mPFC), and the hypothalamus, thus underscoring its role in modulating key aspects of memory and behavior (Fanselow & Dong, 2010; Gergues et. al., 2020; Ciocchi et. al., 2015; Padilla-Coreano et. al., 2016; Jimenez et. al., 2018; Zhou et. al., 2019; Phillips et. al., 2019). These connections have been specifically linked to processing the emotionally valenced components of episodic memories (Fanselow & Dong, 2010). Fittingly, dysfunction in a major hub like the vHPC may lead to deficiencies in numerous cognitive functions including learning, memory, emotional processing, reward-seeking behaviors, and stress responses. Thus, we sought to modulate vCA1 processing by chronically modulating its

activity to test the hypothesis that prolonged network perturbation would lead to cellular and behavioral abnormalities that may be unique to each cell type.

Within the vHPC, a number of studies have focused specifically on neuronal functioning and characterizing the roles of neurons in social, anxiety, goal-directed and fear-related behaviors (Jimenez et. al., 2018, Okuyama et. al., 2016; Jimenez et. al., 2020; Padilla-Coreano et. al., 2016; Ciocchi et. al., 2015; Fanselow & Dong, 2010). Notably, glial cells such as astrocytes, have remained understudied in this ventral axis of the HPC. Astrocytes have primarily been studied as support cells in the brain, aiding in neuronal metabolism, supporting the blood-brain barrier and providing homeostatic regulation of their local environment (Dehouck et. al., 1990; Simard & Nedergard, 2004; Kofuji & Newman, 2004; Paulson & Newman, 1987; Tsacopoulous & Magistretti, 1996; Wallraff et. al., 2006; Rouach et. al., 2008; Figley et. al., 2011). Their active role in synaptic regulation has now been fully recognized, as knowledge of their expression of receptors, transporters and bidirectional communication with neurons has grown (Porter et. al., 1997; Perea & Araque, 2005; Covelo & Araque, 2018; Araque et. al., 2001; Di Castro et. al., 2011; Haydon et. al., 2001; Bezzi & Volterra, 2001). It is now generally thought that astrocytes dynamically respond and modulate circuit activity via calcium-dependent and -independent release of gliotransmitters, such as glutamate, D-serine, and ATP, at the tripartite synapse (Araque et. al., 1999; Perea et. al., 2009; Parpura et. al., 1994; Koizumi et. al., 2005; Fellin et. al., 2004). As astrocytes play a pivotal role in many brain functions, modulation of their structure or activity has a major impact on cognition and behavior (Adamsky et. al., 2018; Kol et. al., 2020; Li et. al., 2020; Mederos et. al., 2021; Martin-Fernandez et. al., 2017; Skucas et. al., 2011). Astrocytes and neurons are heterogenous in their structure and function within and across brain regions, suggesting that perturbation of either cell type may elicit unique behavioral and cellular responses even within the same brain region (Oberheim, Goldman & Nedergaard, 2012; Matyash & Kettenmann, 2010; Buosi et. al., 2017; Zhang & Barres, 2010).

Here, we sought to study the differential effects of chemogenetic activation of the hM3D(Gq) pathway in excitatory neurons (calcium/calmodulin-dependent protein kinase II; CaMKII+) or astrocytes (glial fibrillary acidic protein; GFAP+) in the vHPC, as most studies have identified network hyper- or hypoactivity as a result of disease rather than how onset of this activity may produce pathological brain functioning. In this study, we tested the hypothesis that artificial chronic induction of network hyperactivity in both neuronal and astrocytic groups is sufficient to induce impairments in cognition and behavior, as well as changes in histological markers of cellular stress and inflammation. Our results demonstrate that chronic Gq pathway activation of CaMKII+ neurons or GFAP+ astrocytes in vCA1 across multiple time points is sufficient to induce a variety of changes in behavior and histological markers. Specifically, we found that CaMKII-hM3Dq activation impaired contextual fear acquisition and decreased anxiety-related behaviors. On the other hand, GFAP-hM3Dq activation demonstrated impaired contextual fear acquisition and enhanced fear recall, but no changes in anxiety-related behaviors due to our manipulations alone. For social behaviors, CaMKII-hM3Dq mice exhibited decreased social interaction due to Gq pathway activation, but this was not evident in the GFAP-hM3Dq mice. Interestingly, neuronal manipulation also modified spatial odor memory and novel environment exploration, but astrocytic manipulation did not. Additionally, CaMKII-hM3Dq activation affected the number of microglia in vHPC, but not astrocytes, while GFAP-hM3Dq activation did not modify the number for either

cell type. For glial morphology, only GFAP-hM3Dq activation impacted microglial characteristics, but not astrocytic, and CaMKII-hM3Dq activation did not affect either cell type. Most notably, our manipulation increased the presence of phosphorylated tau (pTau) at the earliest time point with manipulation of both CaMKII+ and GFAP+ cells in vHPC, but was restored over time. Together, this suggests that induction of chronic network perturbation induces differential behavioral effects across cell types. Our study thus provides a mechanistic approach to study how these cell types are uniquely engaged in disorders that have characteristic network dysfunction (e.g. hyper- or hypoactivity) while also adding a more direct role for glia in modulating behavior.

2) Methods.

2.1) Subjects

Wild-type male C57BL/6J mice (P29-35; weight 17-19g; Charles River Labs) were housed in groups of 2-5 mice per cage. The animal facilities (vivarium and behavioral testing rooms) were maintained on a 12:12-hour light cycle (0700-1900). Mice received food and water *ad libitum* before surgery. Following surgery, mice were group-housed with littermates and allowed to recover for a minimum of 4 weeks before experimentation. All animals had their water supply replaced with water-soluble deschloroclozapine dihydrochloride (DCZ) in distilled water (diH2O) solution at a concentration of 3ug/kg/day (17ug/mL). This water was replaced every 5 days to maintain active drug concentrations. All subjects were treated in accord with protocol 201800579 approved by the Institutional Animal Care and Use Committee at Boston University.

2.2) Stereotaxic surgeries

For all surgeries, mice were initially anesthetized with 3.0% isoflurane inhalation during induction and maintained at 1-2% isoflurane inhalation through stereotaxic nose-cone delivery (oxygen 1L/min). Ophthalmic ointment was applied to the eyes to provide adequate lubrication and prevent corneal desiccation. The hair on the scalp above the surgical site was removed using Veet hair removal cream and subsequently cleaned with alternating applications of betadine solution and 70% ethanol. 2.0% lidocaine hydrochloride was injected subcutaneously as local analgesia prior to midsagittal incision of the scalp skin to expose the skull. 0.1mg/kg (5mg/kg) subcutaneous (SQ) dose of meloxicam was administered at the beginning of surgery. All animals received bilateral craniotomies with a 0.5-0.6 mm drill-bit for vCA1 injections. A 10uL Hamilton syringe with an attached 33-gauge beveled needle was slowly lowered to the coordinates of vCA1: -3.16 anteroposterior (AP), ± 3.10 mediolateral (ML) and both -4.25/-4.50 dorsoventral (DV) to cover vertical the axis of vHPC. All coordinates are given relative to bregma (mm). A volume of 150nL (100nL/min) of AAV-CaMKII-hM3Dq-mCherry, AAV-CaMKII-mCherry, AAV5-GFAP-hM3Dq-mCherry or AAV5-GFAP104-hM3Dq-mCherry was bilaterally injected into the vCA1 at both DV coordinates listed above. The needle remained at the target site for 7 minutes post-injection before removal. Incisions were sutured closed using 4/0 Non-absorbable Nylon Monofilament Suture [Brosan]. Following surgery, mice were injected with a 0.1mg/kg intraperitoneal (IP) dose of buprenorphine. They were placed in a recovery cage with a heating pad

until fully recovered from anesthesia. Histological assessment verified bilateral viral targeting and data from off-target injections were not included in analyses.

2.3) Immunohistochemistry

Mice were overdosed with 3% isoflurane and perfused transcardially with cold (4℃) phosphate-buffered saline (PBS) followed by 4% paraformaldehyde (PFA) in PBS. Brains were extracted and kept in PFA at 4℃ for 24-48 hours and transferred to a 30% sucrose in PBS solution. Long-term storage of the brains consisted of transferring to a 0.01% sodium azide in PBS solution until slicing. Brains were sectioned into 50um thick coronal or sagittal sections with a vibratome and collected in cold PBS or 0.01% sodium azide in PBS for long-term storage.

Sections underwent three washes in PBS for 5-10 minutes each to remove the 0.01% sodium azide that they were stored in. Sections were washed three times for 5 minutes each in 0.2% Triton X-100 in PBS (PBST). Sections were blocked for 2 hours at room temperature (RT) in 1% bovine serum albumin (BSA) and 0.2% Triton X-100 in PBS on a shaker. Sections were incubated in primary antibody (1:1000 mouse anti-GFAP [NeuroMab]; 1:1000 rabbit polyclonal anti-Iba1/AIF1 [SySy]; 1:500 polyclonal guinea anti-NeuN/Fox3 [SySy], 1:1000 rabbit polyclonal anti-cFos [SySy], 1:500 mouse monoclonal anti-Phospho-Tau [Ser202, Thr205] [Invitrogen], 1:1000 rabbit polyclonal anti-RFP [Rockland]) made in the same 1% BSA/PBS/Triton X-100 solution at 4℃ for 24 hours. Sections then underwent three washes for 5 minutes each in 0.2% PBST. Sections were incubated in secondary antibodies (1:1000 Alexa Fluor 488 anti-rabbit IgG [Invitrogen]; 1:1000 Alexa Fluor anti-mouse IgG [Invitrogen]; 1:1000 Alexa Fluor 488 anti-guinea IgG [Invitrogen]) for 2 hours at RT. Sections then underwent three more washes in PBST. Sections were then mounted onto microscope slides (VMR International, LLC). Vectashield HardSet Mounting Medium with DAPI (Vector Laboratories, Inc) was applied and slides were coverslipped and allowed to dry for 24 hours at RT. Once dry, slides were sealed with clear nail polish around the edges and stored in a slide box in 4℃. If not mounted immediately, sections were stored in PBS at 4℃.

2.4) Behavioral assays

All behavior assays were conducted during the light cycle of the day (0700-1900) on animals at the 3, 6 and 9 month timepoints. Mice were handled for 3–5 days before all behavioral experiments began. Behavioral assays include open field, zero maze, social interaction, y-maze, spatial odor memory, contextual fear conditioning, recall and extinction tests.

Open field test: An open 61cm x 61cm arena with black plastic walls was used for the open field test, with a red-taped area of 45 cm x 45 cm in the middle delineating “center” from “edges”. A camera was placed above the open field in order to record video of the session. Mice were individually placed into the center of the chamber, and allowed to explore freely for 10 min. At the end of the session, each mouse was placed into a separate cage until all of its cage mates had also gone through the behavioral test. They were all placed back into the home cage once this occurred. An automated video-tracking system, AnyMaze, was used to measure total distance traveled, mean speed, number of entries into the center, and center mean visit time and total time spent in the center.

Zero maze test: The zero maze test is a pharmacologically-validated assay of anxiety in animal models that is based on the natural aversion of mice to elevated, open areas. It is composed of a 44cm wide ring with an outer diameter of 62cm. It contained four equal zones of walled (closed) and unwalled (open) areas. The entire ring is 8cm in height and sits at an elevation of 66cm off the ground. All animals at each timepoint were tested on the same day. Mice were placed in the closed area at the start of a 10 minute session. The following parameters were analyzed: distance traveled, mean speed, time spent in the open area, number of entries into the open area (head and body) and open area mean visit time. The maze was cleaned with 70% ethanol between mice. During the behavioral testing, the lighting levels remained constant and there were no shadows over the surface of the maze.

Social interaction test: An open area (24in x 24in) with black walls was used for the social interaction test. Two inverted wire cups of diameter (4in) and height (4in) were placed in the arena in opposite corners, each set (5in) away from the internal corner of the arena. Black permanent marker was used to draw a circle (6in) on the floor of the area around the outside of the wire cup to demarcate a diameter (1in) larger than that of the cup. A 2-3 month old male conspecific was placed into one wire cup (mouse cup), while the other cup was left empty (empty cup). Each test animal was placed into the middle of the arena and was allowed to freely explore for 10 minutes. A camera was mounted above the arena to record video of behavior for subsequent scoring using AnyMaze. The metrics scored included the total amount of time and number of entries for each region (mouse cup/social target, empty cup). Additionally, total distance traveled was scored.

Y-maze test: The Y-maze is a hippocampal-dependent spatial working memory task that requires mice to use external cues to navigate the identical internal arms. The apparatus consisted of a clear Plexiglass maze with three arms (36.5cm length, 7.5cm width, 12.5cm height) that were intersected at 120 degrees. A mouse was placed at the end of one arm and allowed to move freely through the maze for 10 minutes without any reinforcements, such as food or water. Entries into all arms were noted (center of the body must cross into the arm for a valid entry) and a spontaneous alternation was counted if an animal entered three different arms consecutively without repeat (e.g. ABC, CBA). Percentage of spontaneous alternation was calculated according to the following formula: [(number of alternations)/(total number of arm entries - 1) x 100. To prevent bias in data analysis, the test was carried out in a blind manner by the experimenter and behavior was analyzed blindly in AnyMaze.

Spatial odor memory test: This task was performed exactly as described in Aqrabawi et. al., 2018.

Fear conditioning, recall and extinction:

Fear Conditioning: Fear conditioning for all timepoints took place in mouse conditioning chambers (18.5 x 18.5 x 21.5cm) with metal-panel side walls, plexiglass front and rear walls and a stainless-steel grid floor composed of 16 grid bars (context A). The grid floor was connected to a precision animal shocker set to deliver foot shocks over a time span of 6 minutes or 360s with 1.5 ms 2 second shocks at 120s, 180s, 240s, 300s. A video

camera was mounted to the ceiling of the chamber to record activity and fed into a computer running FreezeFrame software (Actimetrics). This software controlled stimulus presentations and recorded videos from two to four chambers simultaneously. The program determined movement as changes in pixel luminance over a set period of time. Freezing was defined as a bout of 1.25 s or longer without changes in pixel luminance and verified by an experimenter blind to treatment groups. The chambers were cleaned with 70% ethanol solution prior to each animal placement.

Recall: For the recall test, animals were placed into context A for a duration of 5 minutes or 300s 24 hours after fear conditioning.

***Extinction*:** Contextual extinction for all time points took place in context A for 30 minutes or 1800s per session. Three extinction sessions were administered across three consecutive days beginning 24 hours after recall.

2.5) Acute DCZ administration

Mice were subjected to the same surgical protocol described above. After waiting 4 weeks post-surgery for viral expression, mice were injected intraperitoneally (i.p.) with a solution of deschloroclozapine (DCZ) and dimethyl sulfoxide (DMSO) and diluted in sterile saline at a concentration of 10mg/kg (30ug/mL). 90 minutes after injection, mice were time perfused to capture peak cFos protein levels. This was performed with 3 mice per group [CaMKII-hM3Dq, CaMKII-mCherry, GFAP-hM3Dq and GFAP-mCherry] for histological assessment of cFos changes with acute administration of non-water soluble DCZ. It should be noted that mice in the CaMKII-hM3Dq group only appeared behaviorally to experience intense seizure activity. This seizure activity was not observed in any of the other groups during acute administration, nor during our chronic water-soluble administration over the course of 3, 6 and 9 month time points.

2.6) Imaging and cell counting

All coronal and sagittal brain slices were imaged through a Zeiss LSM 800 epifluorescence microscope with a 20x/40x/64x objective using the Zen2.3 software. Full slice images of RFP amplified hM3Dq expression were captured along with zoomed in a 300 x 300 tile (micrometer) z-stack. ROIs for pTau were captured in a 2000 x 1000 image (micrometers) and Z-stack. 3-4 different slices were imaged for each animal for averaging, for each brain region of interest. Images of NeuN, GFAP, and Iba-1 were captured in a 300 x 300 single-tile (micrometers) z-stack. NeuN, GFAP, Iba-1 and cFos counts were performed using Ilastik, a machine-learning-based image analysis tool (Berg et. al., 2019). 3-4 mice per group, with 18 single-tile ROIs covering the vHPC were used for cell counts of NeuN, GFAP and Iba-1. For cFos counts, 3 mice per group with 4 images (1182 x 1756 micrometers) each covering vCA1 were used. Each pyramidal cell layer ROI was hand-traced in ImageJ and cFos counts were normalized to the number of DAPI. Morphological analysis of microglia (Iba1) and astrocytes (GFAP) was performed using 3DMorph, a MATLAB-based tool that analyzes glial morphology from 3-dimensional imaging data (York et. al., 2018). All counts for p-Tau were done with

Image J. The CellCounter tool was used to count individual puncta, positive for p-Tau, within the 2000x1000 tile. These raw counts were then averaged across each animal for statistical analysis.

2.7) Statistical Methods

Data was analyzed using GraphPad Prism. All data were tested for normality using Shapiro-Wilk and Kolmogorov–Smirnov tests and outliers were removed prior to statistical analysis. To analyze differences between groups and across timepoints, we used: Two-way ANOVAs (between-subject factor: Group; within-subject factor: Timepoint). Alpha was set to $p<0.05$. Post-hoc analyses were run using Tukey's-multiple comparisons test with a 95% CI. To analyze differences between groups and across time within a single session we used: Two-way repeated measures (RM) ANOVAs (between-subject factor: Group; within-subject factor: Time). Alpha level was set to 0.05. Post-hoc analyses were run using Šídák's multiple comparisons test with a 95% CI. To analyze differences between groups, we used: Independent t-tests [CaMKII-hM3Dq vs. mCherry; GFAP-hM3Dq vs. mCherry]. Alpha was set to 0.05.

2.8) Reagents and Resources

	SOURCE	**IDENTIFIER**
Experimental Models: Organisms/Strains		
Wild-type male C57Bl/6	Charles River Labs	C57BL/6
Antibodies		
Rabbit polyclonal anti-Iba1/AIF1	SySy	234 003 (catalog #)
Mouse monoclonal anti-GFAP	NeuroMab	75-240 (catalog #)
Guinea polyclonal anti-NeuN/Fox3	SySy	266-004 (catalog #)
Rabbit polyclonal anti-cFos	SySy	226-008 (catalog #)
Rabbit polyclonal anti-RFP	Rockland	600-401-379-RTU
Phospho-Tau [Ser202, Thr205]	Invitrogen	MN1020 (catalog #)
Goat anti rabbit Alexa Fluor 488 Secondary antibody	Invitrogen	A-11008 (catalog #)
Goat anti-guinea pig Alexa Fluor 488 Secondary antibody	Invitrogen	A-11073 (catalog #)
Goat anti-mouse Alexa Fluor 488 Secondary antibody	Invitrogen	A-11001 (catalog #)

Goat anti-rabbit Alexa Fluor 555 Secondary antibody	Invitrogen	A27039 (catalog #)
Chemicals		
Triton X-100	FisherScientific	NC0478124
Paraformaldehyde (PFA)	Sigma-Aldrich	158127-3KG
Bovine serum albumin (BSA)	Sigma-Aldrich	B4287-25G
Deschloroclozapine	HelloBio	HB8555
Deschloroclozapine dihydrochloride	HelloBio	HB9126
Vectashield Hard Set Mounting Medium with DAPI	Vector Laboratories, Inc.	H-1500-10
Software/Programs		
Fiji (ImageJ)		https://fiji.sc/
FreezeFrame4	Coulbourn Instruments	
AnyMaze	Stoelting Co.	
Prism	GraphPad Software	v9.4.1
Ilastik	Berg et. al., 2019	
3DMorph	York et. al., 2018	
Viral Constructs		
AAV-CaMKII-hM3Dq-mCherry	AddGene	50476-AAV9
AAV-CaMKII-mCherry	AddGene	114469-AAV9
AAV5-GFAP-hM3Dq-mCherry	AddGene	50487 -AAV5
AAV5-GFAP104-hM3Dq-mCherry	AddGene	58909-AAV5

3) Results.

3.1) Induction of network dysfunction in neurons or astrocytes across time.

Network dysfunction is an early hallmark of neurodegenerative diseases such as Alzheimer's Disease (AD) both in humans and rodent models (Lauterborn et. al., 2021; Vico Varela et. al., 2019). However, it is

unknown whether chronic activation of astrocytes or neurons in the vHPC may induce behavioral and histological changes related to neurodegeneration in the brains of wild type mice. To address this question, we used chemogenetic methods to chronically activate the hM3D(Gq) pathway in either CaMKII+ neurons or GFAP+ astrocytes in the vCA1 region of the HPC. For the neuronal groups, wild type mice were injected bilaterally with AAV5-CaMKII-hM3D(Gq)-mCherry or control vector AAV5-CaMKII-mCherry to selectively express excitatory DREADD receptors in vCA1 (Figure 1A-B). For the astrocyte groups, C57BL/6 wild type mice were injected bilaterally with AAV9-GFAP-hM3D(Gq)-mCherry or control vector AAV5-GFAP-mCherry to selectively express DREADD receptors in astrocytes within vCA1 as well (Figure 1C-D). Our viruses were robustly expressed in each cell type, as indicated by co-staining with RFP/GFAP+ and RFP/NeuN+ for DREADD receptors and their unique cell markers (Figure 1B,D). After 4 weeks of recovery post-surgery, a potent and water-soluble DREADD ligand, deschloroclozapine dihydrochloride (DCZ) was administered via the animal's daily water to chronically activate the Gq-DREADD receptors of neurons or astrocytes (Figure 1E) (Nagai et. al., 2020). Mice underwent chronic activation for 3, 6 or 9 months, for a total of 12 groups: 3 Month GFAP mCherry and 3 Month GFAP hM3Dq; 3 Month CaMKII mCherry and 3 Month CaMKII hM3Dq; 6 Month GFAP mCherry and 6 Month GFAP hM3Dq; 6 Month CaMKII mCherry and 6 Month CaMKII hM3Dq; 9 Month GFAP mCherry and 9 Month GFAP hM3Dq; 9 Month CaMKII mCherry and and 9 Month CaMKII hM3Dq (Figure 1E). At each group's designated timepoint, mice were subjected to a battery of behavioral tasks including open field, zero maze, social interaction, y-maze, spatial odor memory, CFC, recall and extinction (Figure 1E). Brain tissue was obtained following behavioral testing and was used to perform various histological assessments. Finally, to measure whether our manipulations were killing neurons within the vCA, a confounding variable, we quantified a neuron-specific nuclear marker, NeuN (Figure 1F-I). Analysis of CaMKII-hM3Dq and -mCherry groups revealed no interaction between time point and group for the number of NeuN+ cells, nor did each factor alone contribute to a change in NeuN+ cells (Figure 1F-G)(Two-way ANOVA; Interaction $F(2,12)=0.5069$, $p=0.6147$; Timepoint: $F(2, 12) = 0.5594$, $p=0.5858$; Group: $F(1, 12) = 0.01321$, $p=0.9104$). However, while analysis of the GFAP groups revealed no interaction between time point and group for the number of NeuN+ cells, there was an impact of group (Figure 1H-I)(Two-way ANOVA; Interaction: $F(2, 12) = 0.1286$, $p=0.8805$; Timepoint: $F(2, 12) = 0.8680$, $p=0.4446$; Group: $F(1, 12) = 5.227$, $^{*}p=0.0412$). This suggests that our manipulation of the GFAP-Gq pathway is only mildly affecting the number of NeuN+ cells in a time-independent manner, possibly indicating that there is an initial 'insult' or loss of neurons that does not worsen over time with our chronic Gq activation.

Finally, to confirm the successful acute activation of our Gq-DREADD receptors, we performed intraperitoneal injection of deschloroclozapine (DCZ) and time perfused 90 minutes later to stain for peak cFos protein levels. We hypothesized that cFos levels measured at the time of perfusion in our chronic manipulation mice would show similar expression across groups, as the brain may attempt to restore homeostasis with increases in activity over time, so acute administration was quantified here. We found that across GFAP-hM3Dq and mCherry groups, the administration of exogenous ligand significantly decreased cFos levels (% cFos/DAPI) in vCA1 of the HPC (Supplemental Fig. 7D-F)(Independent two-tailed t-test; $p=0.0438$; $t=2.906$, $df=4$). Additionally, across the CaMKII-hM3Dq and mCherry groups, DCZ administration significantly increased

cFos levels, indicating an increase in neuronal activity (Supplemental Figure 7A-C)(Independent two-tailed t-test; p=0.0438, t=2.906, df=4). This confirms that our DCZ ligand is activating the Gq pathway successfully and induces cellular changes in the brain area of interest. Overall, with chronic administration of DCZ there is no difference in NeuN+ cells in CaMKII-hM3Dq and mCherry groups, but there is an effect of our manipulation in the GFAP-hM3Dq and mCherry groups. Additionally, acute administration of DCZ results in differential cellular changes in vCA1, with an increase in cFos in the CaMKII-hM3Dq group and a decrease in cFos in the GFAP-hM3Dq group compared to their respective controls.

3.2) Chronic Gq activation of CaMKII+ neurons impairs contextual fear acquisition at the 9 month time point.

To test the hypothesis that chronic neuronal Gq activation is sufficient to induce behavioral deficits across all timepoints, we first subjected our mice to CFC, recall, and three days of extinction (Figure 1E). For average percent freezing during CFC, there was a significant interaction between time point [3 month v. 6 month v. 9 month] and group [CaMKII-hM3Dq v. -mCherry] (Two-way ANOVA; Interaction: F (2, 60) = 9.094, p=0.0004; Time point: F (2, 60) = 11.04, p<0.0001; Group: F (1, 60) = 9.496, p=0.0031)(Figure 2A; iv). Subsequent *post hoc* tests demonstrated that 9 month CaMKII-mCherry mice had significantly higher levels of freezing than 3 month CaMKII-mCherry mice (Tukey's; p<0.0001), indicating an increase in fear with aging as shown in previous studies (Yanai & Endo, 2021)(Figure 2A; iv). Most notably, at the 9 month time point, CaMKII-hM3Dq mice had lower overall levels of freezing compared to CaMKII-mCherry controls during CFC (Tukey's, p=0.0013)(Figure 2A; iv). Within the CFC session at 3 months, there were significant differences in freezing over the time bins of the session [seconds; 60, 120, 180, 240, 300, 360], consistent with the natural increase in freezing expected with the repeated shocks administered across the CFC session. However, there were no differences between groups at 3 months [CaMKII-hM3Dq v. -mCherry] or significant interaction effect between the time bins and the groups on freezing levels during CFC (Two-way ANOVA RM; Interaction: F (5, 100) = 1.123, p=0.3532; Time: F (3.377, 67.55) = 71.55, p<0.0001; Group: F (1, 20) = 2.595, p=0.1229; Subject: F (20, 100) = 3.404, p<0.0001)(Figure 2A; i). Within the CFC session at 6 months, there were differences in freezing dependent on time bins similar to the 3 month mice, as well as general increased freezing levels in the CaMKII-mCherry compared to the CaMKII-hM3Dq experimental group. Further, there was no interaction between the time bins and groups (Two-way ANOVA RM; Interaction: F (5, 110) = 1.529, p=0.1866; Time: F (3.017, 66.38) = 70.03, p<0.0001; Group: F (1, 22) = 5.968, p=0.0231; Subject: F (22, 110) = 2.581, p=0.0006)(Figure 2A; ii). Finally, for 9 months, there was a significant interaction between time and group within session for CFC (Two-way ANOVA RM; Interaction: F (5, 90) = 2.484, p=0.0373; Time: F (3.214, 57.84) = 58.85, p<0.0001, F (1, 18) = 15.93, p=0.0009, Subject: F (18, 90) = 2.771, p=0.0008)(Figure 2A; iii). *Post hoc* multiple comparisons revealed that this was driven by lower levels of freezing in the CaMKII-hM3Dq group at the 180, 240 and 360 second time bins during CFC (Šidák multiple comparisons: 180: p<0.0001; 240: p=0.0044; 360: p=0.0168)(Figure 2A; iii).

For contextual recall, the average percent freezing differed across time points but had no significant interaction between those time points and group [CaMKII-hM3Dq and -mCherry], suggesting that aging alone

is increasing freezing levels (Two-way ANOVA; Interaction: F (2, 60) = 2.327, p=0.1064; Timepoint: F (2, 60) = 9.508, p=0.0003; Group: F (1, 60) = 0.8738, p=0.3536)(Figure 2B; iv). Within the recall session at 3 and 6 months, there were significant differences in freezing dependent on time bin but no interaction between time bins and group, as expected with a decrease in freezing within extinction sessions (Figure 2B; i, ii) (3 month: Two-way ANOVA RM; Interaction: F (4, 80) = 0.9819, p=0.4223; Time: F (3.089, 61.79) = 10.53, p<0.0001; Group: F (1, 20) = 0.4380, p=0.5157; Subject: F (20, 80) = 7.617, p<0.0001; 6 month: Two-way ANOVA RM; Interaction: F (4, 88) = 1.979, p=0.1046; Time: F (3.204, 70.49) = 10.38, p<0.0001; Group: F (1, 22) = 0.005898, p=0.9395; Subject: F (22, 88) = 6.368, p<0.0001). Finally, at 9 months there was no interaction between time and group for CaMKII groups, but each factor alone, time and group, affected freezing levels within session (Two-way ANOVA RM; Interaction: F (4, 72) = 0.4759, p=0.7533; Time: F (3.048, 54.87) = 8.045, p=0.0001; Group: F (1, 18) = 5.111, p=0.0364; Subject: F (18, 72) = 5.851, p<0.0001) (Figure 2B; iii).

For extinction day 1, there was an interaction between time point and group for average percent freezing (Two-way ANOVA; Interaction: F (2, 60) = 5.117, p=0.0089; Timepoint: F (2, 60) = 3.857, p=0.0266; Group: F (1, 60) = 0.005006, p=0.9438)(Figure 2C; iv). Subsequent *post hoc* multiple comparisons showed that CaMKII-mCherry mice significantly increased their average freezing levels between the 3 and 9 month time points, indicating an aging effect (Tukey's; p=0.0100) (Figure 2C; iv). Within session at 3 months, there was no interaction between time bin and group, but there were significant differences in freezing depending on time bin and group alone (Figure 2C; i)(Two-way ANOVA RM; Interaction: F (29, 580) = 0.5858, p=0.9601; Time: F (7.717, 154.3) = 2.642, p=0.0105; Group: F (1, 20) = 8.560, p=0.0084; Subject: F (20, 580) = 12.70, p<0.0001). At 6 months, there was no significant interaction between time bin and group, but there was an effect of time only on freezing levels during extinction day 1 (Figure 2C; ii)(Two-way ANOVA RM; Interaction: F (29, 638) = 0.4496, p=0.9948; Time: F (8.852, 194.7) = 6.720, p<0.0001; Group: F (1, 22) = 0.3101, p=0.5832; Subject: F (22, 638) = 19.17, p<0.0001). Finally, at 9 months there was no interaction between time bin and group, nor was freezing impacted by time bin or group alone (Figure 2C; iv)(Mixed-effects model (REML); Time: F (6.259, 110.1) = 2.097, p=0.0565; Group: F (1, 18) = 3.598, p=0.0740; Interaction: F (29, 510) = 1.342, p=0.1121).

For extinction day 2, there was no interaction between time point and group for average percent freezing (Two-way ANOVA; Interaction: F (2, 60) = 2.662; p=0.0781; Time: F (2, 60) = 1.351, p=0.2668; Group: F (1, 60) = 0.001826; p=0.9661) (Figure 2D; iv). At the 3 month time point, there was no interaction between time bin and group, but there were effects of time and group alone on the percent freezing within session (Two-way ANOVA RM; Interaction: F (29, 580) = 1.298, p=0.1385; Time: F (6.958, 139.2) = 3.593, p=0.0014; Group: F (1, 20) = 6.345, p=0.0204; Subject: F (20, 580) = 15.50, p<0.0001) (Figure 2D; i). For 6 months, there was no interaction within session between time bin and group, however, time bin did have an effect on the decrease in freezing during extinction day 2 (Two-way ANOVA RM; Interaction: F (29, 696) = 1.130, p=0.2921; Time: F (5.396, 129.5) = 2.888, p=0.0142; Group: F (1, 24) = 1.313, p=0.2632; Subject: F (24, 696) = 35.67, p<0.0001) (Figure 2D; ii). At 9 months there was a significant interaction between time bin and group on extinction day 2, as well as an effect of time bin alone on freezing levels within session (Two-way ANOVA RM; Interaction: F (29, 522) = 1.918, p=0.0031; Time: F (6.146, 110.6) = 2.383, p=0.0322; Group: F

(1, 18) = 0.1419, p=0.7108; Subject: F (18, 522) = 16.26, p<0.0001)(Figure 2D; iii). *Post-hoc* multiple comparisons did not reveal pairwise differences across groups for each time bin that would describe this variance.

For extinction day 3, there was no interaction between time point and group, but there was an effect of time point on average freezing levels (Two-way ANOVA; Interaction: F (2, 60) = 2.147, p=0.1257; Timepoint: F (2, 60) = 7.099, p=0.0017; Group: F (1, 60) = 0.006334, p=0.9368) (Figure 2E; iv). Within the session, there was no significant interaction between time bin and group for the 3 and 9 month CaMKII-mCherry and hM3Dq mice (Two-way ANOVA RM; [3 Month: Interaction: F (29, 580) = 0.5950, p=0.9557; Time: F (4.761, 95.23) = 1.417, p=0.2273; Group: F (1, 20) = 3.648, p=0.0706; Subject: F (20, 580) = 14.34, p<0.0001][9 Month: Interaction: F (29, 522) = 0.7420, p=0.8353; Time: F (7.702, 138.6) = 1.332, p=0.2345; Group: F (1, 18) = 0.06444, p=0.8025; Subject: F (18, 522) = 19.96, p<0.0001) (Figure 2E; i, iii). However, at 6 months there was an interaction between time bin and group, suggesting that our manipulation is significantly decreasing freezing levels in conjunction with an expected decrease in fear during extinction (Two-way ANOVA RM; Interaction: F (29, 638) = 1.583, p=0.0277; Time: F (6.744, 148.4) = 3.160, p=0.0043; Group: F (1, 22) = 2.086, p=0.1627; Subject: F (22, 638) = 27.14, p<0.0001)(Figure 2E; ii). *Post hoc* analysis did not reveal any pairwise differences [CaMKII-mCherry vs. hM3Dq] at each time bin.

When observing behavior across days, CaMKII-hM3Dq and mCherry groups had no interaction between day [fear conditioning, recall, extinction days 1-3] and group [CaMKII-hM3Dq and mCherry] at the 3, 6 and 9 month time points. However, at the 3 and 9 month time points, there were individual effects of both day and group, suggesting that our manipulation of the Gq pathway was impacting average freezing levels. Additionally, at the 6 month time point, there was an effect of day only, suggesting that our experimental manipulation was not having an impact at this time point (Two-way ANOVA RM; [3 Month: Interaction: F (4, 80) = 1.166, p=0.3320; Day: F (2.954, 59.08) = 42.66, p<0.0001; Group: F (1, 20) = 5.443, p=0.0302; Subject: F (20, 80) = 5.297, p<0.0001][6 month: Interaction: F (4, 88) = 0.5515, p=0.6984; Day: F (4, 88) = 25.72, p<0.0001; Group: F (1, 22) = 2.571, p=0.1231; Subject: F (22, 88) = 1.949, p=0.0153][9 month: Interaction: F (4, 72) = 1.580, p=0.1888; Day: F (2.640, 47.52) = 28.45, p<0.0001; Group: F (1, 18) = 11.43, p=0.0033; Subject: F (18, 72) = 1.158, p=0.3188])(Supp. Figure 3D-F).

In summary, our CaMKII-hM3Dq manipulation significantly decreased freezing levels during CFC compared to CaMKII-mCherry controls. During acquisition, we also observed an increase in fear with aging in the 3 vs. 9 month CaMKII-mCherry groups. For recall, we observed a change in average freezing due to aging alone. Our manipulation affected recall behavior at the 9 month time point only, with both time bin and group contributing individually. For extinction day 1, we observed an increase in freezing with aging, as evidenced in 3 vs. 9 month CaMKII-mCherry mice across time. At 3 months, there was an increase in freezing within the extinction day 1 session in the CaMKII-hM3Dq group compared to controls, as well as across time bins. At 6 months, only the time bin contributed to differences in freezing within the session, and at 9 months there was no impact of group or time bin on freezing levels within session. For extinction day 2, there were no differences in average freezing across groups. However, we observed an increase in freezing at 3 months, due to our manipulation and time bin within the session. At 6 months, only the time bin contributed to a change in freezing during extinction day 2. At 9 months, we observed a decrease in freezing within the session due to

group and time bin. Finally, for extinction day 3 we observed significant differences in freezing across time points, indicating an effect of aging across both groups, but no overall impact of our Gq manipulation. Specifically, at 6 months we find a decrease in freezing within session for our CaMKII-hM3Dq group, but no differences within session for 3 or 9 month time points. Overall, our neuronal-targeted Gq manipulation produces differential effects on contextual fear acquisition, recall and extinction behaviors, suggesting that normal functioning of excitatory neurons in vHPC is necessary for proper fear acquisition and maintenance.

3.3) Gq pathway activation in GFAP+ astrocytes impairs acquisition and enhances recall of contextual fear memory at the 9 month time point.

Next, to test the hypothesis that chronic astrocytic Gq activation is sufficient to induce behavioral deficits across all timepoints, we subjected our mice to CFC, recall, and three days of extinction (Figure 1E). For fear conditioning, there was an interaction between group and time point for average freezing (Two-way ANOVA; Interaction: $F(2, 46) = 13.46$, $p<0.0001$; Timepoint: $F(2, 46) = 0.8634$, $p=0.4284$; Group: $F(1, 46) = 10.87$, $p=0.0019$)(Figure 3A; iv). *Post hoc* multiple comparisons revealed that 3 vs. 9 month GFAP-mCherry mice displayed significantly increased freezing levels with aging (Tukey's; $p=0.0006$)(Figure 3A; iv). Additionally, 6 vs. 9 month GFAP-hM3Dq mice displayed a significant decrease in freezing with aging (Tukey's; $p=0.0412$)(Figure 3A; iv). At the 9 month time point, hM3Dq+ mice had significantly lower levels of freezing during CFC than controls (Tukey's; $p<0.0001$)(Figure 3A; iv). Within the session, mice at 3 months showed no interaction between time bin and group. On the other hand, each factor alone had an effect on freezing level during CFC (Two-way ANOVA RM; Interaction: $F(5, 115) = 1.201$, $p=0.3133$; Time: $F(5, 115) = 135.1$, $p<0.0001$; Group: $F(1, 23) = 8.509$, $p=0.0078$; Mouse: $F(23, 115) = 2.421$, $p=0.0011$)(Figure 3A; i). At 6 months, there was no interaction between time bin and group, but there was an effect of time bin alone that is expected as mice acquire fear successfully within session (Two-way ANOVA RM; Interaction: $F(5, 85) = 1.054$, $p=0.3916$; Time: $F(3.198, 54.36) = 71.62$, $p<0.0001$; Group: $F(1, 17) = 0.1673$, $p=0.6877$; Mouse: $F(17, 85) = 3.188$, $p=0.0002$)(Figure 3A; ii). At 9 months, there was a significant interaction between time bin and group within session, suggesting that our manipulation decreased freezing levels (Two-way ANOVA RM; Interaction: $F(5, 40) = 5.880$, $p=0.0004$; Time: $F(2.960, 23.68) = 22.44$, $p<0.0001$; Group: $F(1, 8) = 22.23$, $p=0.0015$; Mouse: $F(8, 40) = 2.412$, $p=0.0315$)(Figure 3A; iii). *Post hoc* analysis revealed that mice in the GFAP-hM3Dq group had lower levels of freezing at the 300 and 360 second time bins (Tukey's; 300s: $p=0.0023$; 360s: $p=0.0095$)(Figure 3A; iii).

For recall, there was a significant interaction between time point and group, suggesting that our manipulation and aging impacted average freezing levels (Two-way ANOVA; Interaction: $F(2, 44) = 5.366$, $p=0.0082$; Timepoint: $F(2, 44) = 3.199$, $p=0.0504$; Group: $F(1, 44) = 1.810$, $p=0.1854$)(Figure 3B; iv). *Post hoc* analysis revealed that 6 vs. 9 month GFAP-mCherry mice decreased freezing levels with aging (Tukey's: $p=0.0066$)(Figure 3B; iv). On the other hand, at the 9 month time point the GFAP-hM3Dq mice exhibited significantly higher freezing levels compared to controls on average (Tukey's: $p=0.0369$)(Figure 3B; iv). Within session at 3 and 6 months, there was no interaction between time bin and group, but there was an effect of time bin alone (Two-way ANOVA RM; [3 Month: Interaction: $F(4, 92) = 0.5448$, $p=0.7033$; Time: $F(4, 92) =$

12.54, p <0.000; Group: F (1, 23) = 0.02859, p=0.867; Mouse: F (23, 92) = 8.422, p<0.0001)][6 Month: Interaction: F (4, 52) = 0.3647, p=0.8326; Time: F (2.512, 32.65) = 13.56, p<0.0001; Group: F (1, 13) = 1.326, p=0.2702; Mouse: F (13, 52) = 7.540, p<0.0001])(Figure 3B; i, ii). This suggests that GFAP-hM3Dq and mCherry mice displayed comparable levels of freezing within session, with our manipulation not affecting recall behaviors at these earlier time points. Finally, at 9 months there was no interaction between time bin and group within session, but group alone did have an effect on freezing levels within the recall session (Two-way ANOVA RM; Interaction: F (4, 32) = 1.083, p=0.3814; Time: F (2.436, 19.49) = 2.898, p=0.0704; Group: F (1, 8) = 18.14, p=0.0028; Mouse: F (8, 32) = 4.094, p=0.0019)(Figure 3B; iii). This suggests that our manipulation of the GFAP-Gq pathway is increasing freezing levels during recall at 9 months as compared to mCherry controls.

We observed no significant interaction between time point and group for extinction day 1, only an effect of time point alone, suggesting that only aging contributed to the variance in freezing behavior (Two-way ANOVA; Interaction: F (2, 48) = 3.054, p=0.0564; Timepoint: F (2, 48) = 6.726, p=0.0027; Group: F (1, 48) = 0.3569, p=0.5530)(Figure 3C; iv). Within session at 3 months, there was no interaction between time bin and group, however each factor contributed independently to freezing levels during extinction (Two-way ANOVA RM; Interaction: F (29, 690) = 0.6285, p=0.9370; Time: F (29, 690) = 2.529, p<0.0001; Group: F (1, 690) = 63.51, p<0.0001)(Figure 3C; i). At 6 and 9 months, there was no interaction between time bin and group, but our manipulation (group) alone contributed significantly to freezing levels within session (Two-way ANOVA; [6 Months: Interaction: F (29, 510) = 0.5914, p=0.9571; Time: F (29, 510) = 0.9590, p=0.5292; Group: F (1, 510) = 14.36, p=0.0002][9 Months: Interaction: F (29, 236) = 0.3020, p=0.9998; Time: F (29, 236) = 0.6476, p=0.9191; Group: F (1, 236) = 40.08, p<0.0001])(Figure 3C; ii, iii). For extinction day 2, there was no interaction between group and time point, but there was an effect of time point alone that decreased freezing levels with aging (Two-way ANOVA; Interaction: F (2, 48) = 1.688, p=0.1958; Timepoint: F (2, 48) = 4.132, p=0.0221; Group: F (1, 48) = 0.03197, p=0.8588)(Figure 3D; iv). Within session at 3 months, there was no interaction between time bin and group, but time bin alone had an effect on a decrease in freezing across extinction (Two-way ANOVA RM; Interaction: F (29, 667) = 0.9633, p=0.5225; Time: F (29, 667) = 1.735, p=0.0102; Group: F (1, 23) = 2.356, p=0.1385; Mouse: F (23, 667) = 29.95, p<0.0001)(Figure 3D; i). At 6 and 9 months, there was no significant interaction between time bin and group, only an effect of time bin for the 9 month time point (Two-way ANOVA RM; [6 Month: Interaction: F (29, 493) = 0.9984, p=0.4704; Time: F (6.484, 110.2) = 2.020, p=0.0637; Group": F (1, 17) = 0.2175, p=0.6468; Mouse: F (17, 493) = 23.34, p<0.0001)(Figure 3D, ii-iii).

Finally, for extinction day 3 there was no significant interaction between group and time point for average freezing levels, suggesting that age nor our manipulation impacted behavior (Two-way ANOVA RM; Interaction: F (2, 48) = 2.782, p=0.0719; Timepoint: F (2, 48) = 2.116, p=0.1316; Group: F (1, 48) = 1.314, p=0.2574)(Figure 3E; iv). At 3 months, there was no interaction between time bin and group within session, but the time bin factor had an effect on the decrease in freezing level (Two-way ANOVA RM; Interaction: F (29, 667) = 1.078, p=0.3573; Time: F (6.706, 154.2) = 2.136, p=0.0455; Group: F (1, 23) = 1.622, p=0.2155; Mouse: F (23, 667) = 16.12, p<0.0001)(Figure 3E; i). However, at 6 months there was an interaction between group and time bin on freezing levels within session, suggesting that our manipulation had an effect in the GFAP-hM3Dq

group (Two-way ANOVA RM; Interaction: F (29, 493) = 1.857, p=0.0048; Time: F (7.353, 125.0) = 1.200, p=0.3067; Group: F (1, 17) = 2.354, p=0.1433; Mouse: F (17, 493) = 16.51, p<0.0001)(Figure 3E; ii). Finally, at 9 months there was no interaction between time bin and group (Two-way ANOVA RM; Interaction: F (29, 232) = 1.399, p=0.0923; Time: F (3.166, 25.33) = 1.225, p=0.3220; Group: F (1, 8) = 2.431, p=0.1575; Mouse: F (8, 232) = 20.31, p<0.0001)(Figure 3E, iii).

For GFAP-hM3Dq and mCherry groups, there was no interaction between day and group at the 3 and 6 month time points. However, there was an effect of day alone, suggesting that our manipulation was not having any effect on learning (Mixed-effects model (REML): [3 Month: Interaction: F (4, 89) = 2.096, p=0.0879; Day; F (4, 89) = 11.18, p<0.0001; Group: F (1, 23) = 2.859, p=0.1044][6 Month: Interaction: F (4, 81) = 1.342, p=0.2617; Day: F (4, 81) = 14.72, p<0.0001; Group: F (1, 81) = 0.4120, p=0.5228])(Supp. Figure 3A-B). Most interestingly, there was a significant interaction between day and group at the 9 month time point for GFAP-hM3Dq and mCherry groups (Two-way ANOVA RM; Interaction: F (4, 32) = 11.24, p<0.0001; Day: F (4, 32) = 17.07, p<0.0001; Group: F (1, 8) = 3.936, p=0.0826; Subject: F (8, 32) = 1.216, p=0.3214)(Supp. Figure 3C). Further analysis revealed significant differences in freezing between groups at the 9 month time point for the fear conditioning (Tukey's: p=0.0011) and recall (Tukey's: p=0.0002) days (Supp. Figure 3C).

In summary, our GFAP-hM3Dq manipulation significantly decreased freezing levels during contextual fear acquisition compared to mCherry controls at 9 months. During acquisition, we also observed an increase in fear with aging in the 3 vs. 9 month GFAP-mCherry groups. Within the 3 month CFC session, we observed an increase in freezing in the GFAP-hM3Dq group, but at the 9 month session we observed a decrease in freezing levels compared to controls. For recall, we observed a significant increase in freezing levels in our GFAP-hM3Dq experimental group at the 9 month time point. Additionally, we saw a decrease in freezing levels across the 6 and 9 month GFAP-mCherry groups, suggesting an effect of aging. Within the session for recall, there was an effect of our manipulation on freezing levels at the 9 months time point. For extinction day 1, we observed a decrease in percent freezing across time, indicating an effect of aging alone. Interestingly, within extinction day 1 sessions at the 3 and 6 month time points, we observed an increase in freezing due to our manipulation, but a decrease in freezing at the 9 month time point. For extinction day 2, we observed a decrease in freezing across time points, indicating an effect of aging alone. Finally, at 6 months there was only a decrease in freezing levels within session for extinction day 3. Overall, our manipulation of GFAP+ astrocytes in vHPC induced significant behavioral changes in fear acquisition and maintenance at the 9 month time point primarily.

3.4) Chronic Gq activation of neurons induces behavioral changes in locomotor and anxiety-related behaviors.

The open field and elevated zero maze are tasks that are classically used to measure locomotor activity and anxiety-like behaviors (Seibenhener & Wooten, 2015; Tucker & McCabe, 2017). To test our hypothesis that chronic activation of the Gq pathway in neurons will exhibit disrupted anxiety-like behaviors, we subjected the mice to these tasks on consecutive days (Figure 1E). For open field, CaMKII-hM3Dq and mCherry mice had no significant interaction between time point and group in the total distance traveled, time spent in center, and

number of entries to the center (Figure 4A, C-D). However, each factor alone (i.e. group and time point) individually contributed to all three of these metrics (Two-way ANOVA; [Distance traveled: Interaction: $F(2, 65) = 0.5961$, $p=0.5540$; Timepoint: $F(2, 65) = 3.437$, $p=0.0381$; Group: $F(1, 65) = 6.664$, $p=0.0121$][Center time: Interaction: $F(2, 56) = 0.5527$, $p=0.5785$; Timepoint: $F(2, 56) = 13.97$, $p<0.0001$; Group: $F(1, 56) = 7.767$, $p=0.0073$][Center entries: Interaction: $F(2, 58) = 1.353$, $p=0.2664$; Timepoint: $F(2, 58) = 8.707$, $p=0.0005$; Group: $F(1, 58) = 4.134$, $p=0.0466$]). This suggests that both aging and our Gq pathway manipulation is driving significant differences in anxiety-related behaviors. Mean speed in the open field demonstrated no interaction between time point and group, but group alone contributed to a modification in behavior at each time point (Two-way ANOVA; Interaction: $F(2, 62) = 0.2549$, $p=0.7758$; Time point: $F(2, 62) = 3.103$, $p=0.0519$; Group: $F(1, 62) = 4.937$, $p=0.0299$)(Figure 4B). Further, there was no significant interaction between time point and group for center mean visit time (Two-way ANOVA; Interaction: $F(2, 57) = 1.168$, $p=0.3182$; Timepoint: $F(2, 57) = 1.972$, $p=0.1486$; Group: $F(1, 57) = 2.985$, $p=0.08950$)(Figure 4E). This suggests that the combination of aging and the manipulation of the CaMKII-Gq pathway drives significant differences in anxiety-related behaviors.

In the elevated zero maze, there was no significant interaction between time point and group for total distance traveled, mean speed, body entries into the open area, or head entries into the open area. However, time point alone had an effect on behavior for all of these metrics, with each measure decreasing across aging (Two-way ANOVA; [Distance traveled: Interaction: $F(2, 62) = 0.6878$, $p=0.5065$; Timepoint: $F(2, 62) = 27.98$, $p<0.0001$; Group: $F(1, 62) = 0.2502$, $p=0.6187$][Mean speed: Interaction: $F(2, 62) = 0.7047$, $p=0.4982$; Timepoint: $F(2, 62) = 27.25$, $p<0.0001$; Group: $F(1, 62) = 0.2245$, $p=0.6373$][Open area body entries: Interaction: $F(2, 62) = 0.5662$, $p=0.5706$; Timepoint: $F(2, 62) = 19.92$, $p<0.0001$; Group: $F(1, 62) = 0.04116$, $p=0.8399$][Open area head entries: Interaction: $F(2, 62) = 2.369$, $p=0.1020$; Timepoint: $F(2, 62) = 60.87$, $p<0.0001$; Group: $F(1, 62) = 1.614$, $p=0.2086$])(Figure 4F-G, I, K). Interestingly, for the time spent in the open area and mean visit time there was an interaction between both time point and our group manipulation (Two-way ANOVA; [Open area time: Interaction: $F(2, 59) = 3.564$, $p=0.0346$; Timepoint: $F(2, 59) = 2.028$, $p=0.1406$; Group: $F(1, 59) = 2.514$, $p=0.1182$][Open area mean visit time: Interaction: $F(2, 61) = 6.537$, $p=0.0027$; Timepoint: $F(2, 61) = 14.68$, $p<0.0001$; Group: $F(1, 61) = 4.244$, $p=0.0437$])(Figure 4H, J). *Post hoc* multiple comparisons revealed significant pairwise increases across 3 vs. 9 month CaMKII-hM3Dq (Tukey's: $p<0.0001$) and the 6 vs. 9 month CaMKII-hM3Dq groups (Tukey's: $p<0.0001$), with open area mean visit time increasing with age (Figure 4J). Most interestingly, our manipulation of the Gq pathway induced a significant increase in the mean visit time to the open area of the zero maze at the 9 month time point when comparing CaMKII-hM3Dq and mCherry groups (Tukey's: $p=0.0148$)(Figure 4J). Additionally, there was an increase in the mean visit time to the open area at 9 months in the experimental compared to the control group. Finally, we observe normal aging changes in distance traveled, mean speed, body entries and head entries to the open area, indicating an increase in anxiety with age (Yanai & Endo, 2021). Overall, CaMKII Gq activation had a combinatory effect on anxiety-related behaviors with age, as evidenced by increases in mean visit time and time spent in the open area of the zero maze across time points in the hM3Dq group.

3.5) Chronic Gq activation of astrocytes induces behavioral changes in locomotor and anxiety-related behaviors.

We tested the hypothesis that chronic modulation of the Gq pathway in astrocytes would induce changes in anxiety-related behaviors. (Figure 1E). For open field, GFAP-hM3Dq and mCherry mice showed no significant interaction between time point and group in the total distance traveled and mean speed. However, there was an effect of time point alone for both measures, indicating a decrease in distance traveled and mean speed with aging that is shown in previous literature (Two-way ANOVA; [Distance Traveled: Interaction: $F(2, 47) = 2.190$, $p=0.1232$; Timepoint: $F(2, 47) = 24.51$, $p<0.0001$; Group: $F(1, 47) = 1.731$, $p=0.1946$][Mean Speed: Interaction: $F(2, 47) = 2.186$, $p=0.1237$; Timepoint: $F(2, 47) = 24.53$, $p<0.0001$; Group: $F(1, 47) = 1.762$, $p=0.1907$)(Figure 5A-B)(Yanai & Endo, 2021). For time spent in the open field, there was no interaction between time point and group, but each factor alone contributed to an increase in the amount of time spent by the GFAP-hM3Dq group (Two-way ANOVA; Interaction: $F(2, 46) = 2.851$, $p=0.0680$; Timepoint: $F(2, 46) = 9.747$, $p=0.0003$; Group: $F(1, 46) = 11.77$, $p=0.0013$)(Figure 5C). For the number of entries into the center of the open field, there was no interaction between time point and group (Two-way ANOVA; Interaction: $F(2, 53) = 0.8499$, $p=0.4333$; Timepoint: $F(2, 53) = 1.065$, $p=0.3521$; Group: $F(1, 53) = 0.2607$, $p=0.6117$)(Figure 5D). Finally, for the mean visit time to the center of the open field, there was no interaction between time point and group, but group alone contributed to the increase in the experimental group across all time points (Two-way ANOVA; Interaction: $F(2, 42) = 0.8220$, $p=0.4465$; Timepoint: $F(2, 42) = 0.2008$, $p=0.8189$; Group: $F(1, 42) = 10.58$, $p=0.0023$)(Figure 5E). In summary, there was an expected decrease in distance traveled and mean speed with aging. Our manipulation of the Gq pathway in GFAP+ cells induced changes in mean visit time and time spent in the center of the open field that when compounded by aging changed the animal's anxiety-related behaviors.

For elevated zero maze, GFAP-hM3Dq and mCherry mice showed no significant interaction between time point and group in the total distance traveled, mean speed, time spent in the open area, number of body entries into the open area, number of head entries into the open area, or mean visit time to the open area (Two-way ANOVA; [Distance Traveled: Interaction: $F(2, 48) = 1.413$, $p=0.2535$; Timepoint: $F(2, 48) = 5.315$, $p=0.0082$; Group: $F(1, 48) = 1.260$, $p=0.2672$][Mean Speed: Interaction: $F(2, 48) = 1.374$, $p=0.2628$; Timepoint: $F(2, 48) = 5.097$, $p=0.0098$; Group: $F(1, 48) = 1.170$, $p=0.2848$][Open Area Time: Interaction: $F(2, 46) = 0.5288$, $p=0.5929$; Timepoint: $F(2, 46) = 0.9203$, $p=0.4056$; Group: $F(1, 46) = 0.01378$, $p=0.9071$][Open Area Body Entries: Interaction: $F(2, 47) = 0.9588$, $p=0.3907$; Timepoint: $F(2, 47) = 4.648$, $p=0.0144$; Group: $F(1, 47) = 1.581$, $p=0.2148$][Open Area Head Entries: Interaction: $F(2, 46) = 0.4991$, $p=0.6103$; Timepoint: $F(2, 46) = 16.01$, $p<0.0001$; Group: $F(1, 46) = 1.134$, $p=0.2925$][Open Area Mean Visit Time: Interaction: $F(2, 47) = 0.1068$, $p=0.8989$; Timepoint: $F(2, 47) = 14.65$, $p<0.0001$; Group: $F(1, 47) = 0.01249$, $p=0.9115$])(Figure 5F-K). However, all of these metrics, except time spent in the open area, had an effect of time point, suggesting that although our manipulation of GFAP-Gq did not impact behavior in this anxiety task, however, aging did play a role. Specifically, aging had an impact on decreased distance traveled, mean speed, open area body entries and open area head entries. There was an increase in open area mean visit time with aging alone due to these effects.

3.6) Chronic Gq activation decreases social behaviors in CaMKII, but not in GFAP, groups.

To assess how social behaviors are impacted by our manipulation, we performed a social interaction test by placing the subject mouse in an open arena with a cup containing a male mouse or an empty cup for a 10 minute session. For CaMKII-hM3Dq and mCherry mice, there was no interaction between time point and group for total distance traveled, head time spent at the empty cup, or the number of head entries into the empty cup area. However, these metrics were all impacted by an effect of time point alone, suggesting that aging is contributing to these behavioral changes (Two-way ANOVA; [Distance traveled: Interaction: $F(2, 59) = 1.447$, $p=0.2435$; Timepoint: $F(2, 59) = 69.58$, $p<0.0001$; Group: $F(1, 59) = 0.1835$, $p=0.6699$][Empty cup head time: Interaction: $F(2, 59) = 2.514$, $p=0.0896$; Time point: $F(2, 59) = 13.96$, $p<0.0001$; Group: $F(1, 59) = 0.0005010$, $p=0.9822$][Empty cup mean visit time: Interaction: $F(2, 55) = 0.8991$, $p=0.4128$; Timepoint: $F(2, 55) = 30.29$, $p<0.0001$; Group: $F(1, 55) = 0.7430$, $p=0.3924$])(Supp. Figure 2D-F). Interestingly, for the number of head entries into the mouse cup (i.e. social target), there was a significant interaction between time point and group (Two-way ANOVA; Interaction: $F(2, 59) = 6.145$, $p=0.0038$; Timepoint: $F(2, 59) = 35.11$, $p<0.0001$; Group: $F(1, 59) = 0.4773$, $p=0.4924$)(Supp. Figure 2A). *Post hoc* analysis revealed significant decreases in the number of head entries into the mouse cup between 3 vs. 9 month CaMKII-mCherry (Tukey's: $p<0.0001$), 6 v. 9 month CaMKII-mCherry (Tukey's: $p<0.0001$), 3 vs. 9 month CaMKII-hM3Dq (Tukey's: $p=0.0002$), and 6 vs. 9 month CaMKII-hM3Dq (Tukey's: $p=0.0176$) groups (Supp. Figure 2A). Most notably, there was a significant decrease in the number of head entries into the mouse cup at the 6 month time point between our CaMKII-hM3Dq and mCherry groups (Tukey's: $p=0.0391$)(Supp. Figure 2A). Finally, for the total amount of head time and mean visit time to the mouse cup, as well as the mean visit time to the empty cup, there was no significant interaction between time point and group (Two-way ANOVA; [Mouse cup head time: Interaction: $F(2, 56) = 1.056$, $p=0.3547$; Time point: $F(2, 56) = 0.5529$, $p=0.5784$; Group: $F(1, 56) = 0.8246$, $p=0.3677$][Mouse cup mean visit time: Interaction: $F(2, 55) = 1.138$, $p=0.3278$; Timepoint: $F(2, 55) = 2.494$, $p=0.0919$; Group: $F(1, 55) = 3.475$, $p=0.0676$][Empty cup mean visit time: Interaction: $F(2, 52) = 1.333$, $p=0.2727$; Timepoint: $F(2, 52) = 2.111$, $p=0.1314$; Group: $F(1, 52) = 0.7496$, $p=0.3906$])(Supp. Figure 2B-C, G). Overall, we found a significant decrease in the number of entries into the mouse cup area within the 6 month time point, suggesting that these mice may have decreased interest in the social target with our manipulation. There were expected effects of aging, such as decreased distance traveled, as well as general decreased interest in social targets (Shoji et al, 2016; Oizumi et al, 2019; Yanai & Endo, 2021).

For GFAP-hM3Dq and mCherry mice, there was no significant interaction between time point and group for total distance traveled, mean speed, head time at the mouse cup (i.e. social target) or empty cup (i.e. control), head entries into the mouse cup or empty cup zones, or mean visit time to the mouse cup or empty cup during social interaction. However, we did observe significant effects of aging across all metrics, except in mean visit time to the empty cup (Two-way ANOVA; [Distance traveled: Interaction: $F(2, 46) = 1.791$, $p=0.1782$; Timepoint: $F(2, 46) = 18.51$, $p<0.0001$; Group: $F(1, 46) = 0.7285$, $p=0.3978$][Mean speed: Interaction": $F(2, 45) = 2.046$, $p=0.1411$; Timepoint: $F(2, 45) = 18.32$, $p<0.0001$; Group: $F(1, 45) = 0.4604$, $p=0.5009$][Mouse cup head time: Interaction: $F(2, 42) = 1.829$, $p=0.1731$; Timepoint: $F(2, 42) = 50.83$,

p<0.0001; Group: F (1, 42) = 1.044, p=0.3127][Mouse cup head entries: Interaction: F (2, 44) = 0.9348, p=0.4003; Timepoint: F (2, 44) = 49.18, p<0.0001; Group: F (1, 44) = 0.9721, p=0.3295][Mouse cup mean visit time: Interaction: F (2, 45) = 1.912, p=0.1597; Timepoint: F (2, 45) = 16.24, p<0.0001; Group: F (1, 45) = 1.949, p=0.1696][Empty cup head time: Interaction: F (2, 47) = 0.02273, p=0.9775; Timepoint: F (2, 47) = 3.899, p=0.0271; Group: F (1, 47) = 0.02722, p=0.8697][Empty cup head entries: Interaction: F (2, 47) = 0.3003, p=0.7420; Timepoint: F (2, 47) = 7.689, p=0.0013; Group: F (1, 47) = 0.3428, p=0.5610][Empty cup mean visit time: Interaction: F (2, 46) = 0.4523, p=0.6390; Timepoint: F (2, 46) = 0.8449, p=0.4362; Group: F (1, 46) = 0.8260, p=0.3682])(Supp. Figure 1A-G). Overall, we found no significant changes within each time point between hM3Dq and mCherry groups for social interaction as an effect of our chronic manipulation of astrocytes, only effects of aging alone.

3.7) Spatial odor memory and novel environment exploration behaviors change with chronic Gq manipulation of neurons, but not astrocytes.

Dysfunction of the HPC can negatively impact spatial memory (Clark, Broadbent & Squire, 2009; Broadbent, Squire & Clark, 2004), therefore, we assessed our mice with a spatial odor memory. Our spatial odor memory task relied on the mice recalling the spatial location of a specific odor (orange or almond) within a context A vs. B. The behavioral read-out of this task is a discrimination score: a positive score denotes more time spent exploring the novel odor, a negative score denotes more time spent with the familiar odor and a score of zero indicates equal exploration of both odors. With chronic activation of the Gq pathway in neurons and astrocyte group, we observed no significant interaction between group or time points in the discrimination ratio for spatial odor memory (Two-way ANOVA; [CaMKII-hM3Dq vs. mCherry: Interaction: F (2, 60) = 0.2149, p=0.8072; Timepoint: F (2, 60) = 0.1700, p=0.8441; Group: F (1, 60) = 0.04422, p=0.8342][GFAP-hM3Dq vs. mCherry: Interaction: F (2, 48) = 0.7196, p=0.4921; Timepoint: F (2, 48) = 0.6276, p=0.5382; Group: F (1, 48) = 0.08676, p=0.7696])(Supp. Figure 1J, 2J). Overall, neither Gq activation of neurons or astrocytes in vHPC, nor aging, affected behavior in spatial odor memory.

When exploring a novel environment, rodents generally investigate novel objects and spaces. To assess novel context exploration and quantify putative cognitive deficits, we performed an elevated y-maze test. After introduction into the center of the y-maze, mice freely explore each of three arms (labeled A, B, C). The behavioral output of this task is measured by the percentage of spontaneous alternations and percentage of re-entries into the same arm. A spontaneous alternation is defined as three consecutive entrances into novel arms without repeats (i.e. ABC, CBA). A re-entry is defined as entering the same arm twice in a row (i.e. AA, BB, CC). For chronic activation of CaMKII-specific Gq pathway, there was a significant interaction between group and time point for the percentage of spontaneous alterations (Two-way ANOVA; Interaction: F (2, 60) = 6.655, p=0.0025; Timepoint: F (2, 60) = 12.65, p<0.0001; Group: F (1, 60) = 0.9491, p=0.3339)(Supp. Figure 2H). *Post hoc* analyses revealed that there were significant pairwise differences between the 3 vs. 6 month CaMKII-hM3Dq (Tukey's: p<0.0001) and 3 vs. 9 month CaMKII-hM3Dq groups (Tukey's: p=0.0002)(Supp. Figure 2H). This suggests that our manipulation of CaMKII-specific Gq pathways and aging are interacting to drive this specific effect in y-maze behavior. Additionally, there was no interaction between group and time

point for the number of re-entries in the CaMKII-hM3Dq and control groups. However, there was an independent effect of time point in this behavioral metric, suggesting that aging alone is contributing to a change in y-maze behavior (Two-way ANOVA; Interaction: F (2, 60) = 1.893, p=0.1596; Timepoint: F (2, 60) = 3.878, p=0.0261; Group: F (1, 60) = 0.2529", p=0.6169)(Supp. Figure 2I).

For Gq activation of GFAP+ astrocytes, we observed no significant interaction between group and time point for percentage of spontaneous alternations or number of re-entries. However, there was an individual effect of time point for re-entries, suggesting that aging alone is contributing to a behavioral change in the y-maze (Two-way ANOVA; [Spontaneous alternations; Interaction: F (2, 47) = 1.146, p=0.3265; Timepoint: F (2, 47) = 2.655, p=0.0808; Group: F (1, 47) = 0.07069, p=0.7915][Re-entries; Interaction: F (2, 46) = 1.015, p=0.3705; Timepoint": F (2, 46) = 3.308, p=0.0455; Group: F (1, 46) = 1.946, p=0.1697])(Supp. Figure 1H-I). Overall, chronic activation of neurons compounded with aging impacted behavior in the y-maze. On the other hand, astrocytic activation did not affect the percentage of spontaneous alternations or number of re-entries in the y-maze, only aging played a role in the behavioral changes observed.

3.8) CaMKII-hM3Dq activation changes the number of microglia in vHPC, but not the number of astrocytes. GFAP-hM3Dq activation does not change the number of microglia or astrocytes in vHPC.

As glial cells play a major role in dysfunctional circuit activity in the brain (Liddelow et. al., 2020), we next quantified the cellular changes that our chronic astrocytic or neuronal manipulations induced. To accomplish this, we first quantified the total number of Iba1+ microglia in vCA1 across groups. For CaMKII-hM3Dq and mCherry groups, there was no interaction between time point and group for the number of Iba-1+microglia in vCA1 of the HPC. However, there was an effect of our manipulation of the CaMKII-Gq pathway, suggesting that chronic activation of neurons in this region induces changes in microglial number (Two-way ANOVA; Interaction: F (2, 12) = 1.564, p=0.2492; Time point: F (2, 12) = 1.797, p=0.2077; Group: F (1, 12) = 10.86, p=0.0064)(Figure 6C). On the other hand, for the GFAP-hM3Dq and mCherry groups, there was no interaction between time point and group, nor were there individual effects of either factor on microglial number (Two-way ANOVA; Interaction: F (2, 12) = 0.5945, p=0.5673; Timepoint: F (2, 12) = 1.962, p=0.1831; Group: F (1, 12) = 0.3854, p=0.5463)(Figure 7C). Next, we quantified the total number of GFAP+ astrocytes in vHPC across groups. Across all CaMKII and GFAP groups, there were no significant interactions between time point and group for astrocytic number (Two-way ANOVA; [CaMKII-hM3Dq vs. mCherry: Interaction: F (2, 12) = 0.7052, p=0.5134; Timepoint: F (2, 12) = 3.220, p=0.0759; Group: F (1, 12) = 0.7784, p=0.3950][GFAP-hM3Dq vs. mCherry: Interaction: F (2, 12) = 0.2408, p=0.7897; Timepoint: F (2, 12) = 2.557, p=0.1189; Group: F (1, 12) = 2.672, p=0.1281])(Figure 6J, 7J). Overall, our CaMKII-hM3Dq manipulation induced significant changes in microglial number in vHPC, but did not affect astrocytic number. Additionally, our GFAP-hM3Dq manipulation did not impact microglial or astrocytic number.

3.9) GFAP-hM3Dq activation impacted microglial morphology, but CaMKII-hM3Dq did not.

To further analyze the impact of our CaMKII or GFAP Gq pathway activation, we performed morphological analysis of microglia in vHPC. For CaMKII-hM3Dq and mCherry groups, there was no

significant interaction between time point and group for microglial cell territory volume, cell volume, ramification index or average branch length (Two-way ANOVA; [Cell territory volume: Interaction: F (2, 12) = 0.7040, p=0.5139; Timepoint: F (2, 12) = 1.240, p=0.3239; Group: F (1, 12) = 2.244, p=0.1600][Cell volume: Interaction: F (2, 12) = 0.9601, p=0.4104; Timepoint: F (2, 12) = 0.06630, p=0.9362; Group: F (1, 12) = 1.423, p=0.2560][Ramification index: Interaction: F (2, 12) = 1.217, p=0.3303; Timepoint: F (2, 12) = 2.981, p=0.0889; Group: F (1, 12) = 0.02767, p=0.8707][Avg branch length: Interaction: F (2, 12) = 0.08429, p=0.9197; Timepoint: F (2, 12) = 2.464, p=0.1269; Group: F (1, 12) = 0.2552, p=0.6226])(Figure 6D-G). Additionally, for microglia there were no interactions between time point and group for the number of endpoints, minimum branch length, maximum branch length or number of branch points, but there was an effect of aging for the number of branch points and endpoints (Two-way ANOVA; [Num Endpoints: Interaction: F (2, 12) = 0.1217, p=0.8865; Timepoint: F (2, 12) = 4.365, p=0.0376; Group: F (1, 12) = 0.3498, p=0.5652][Min branch length: Interaction: F (2, 12) = 0.4630, p=0.6402; Timepoint: F (2, 12) = 0.6621, p=0.5336; Group: F (1, 12) = 0.1133, p=0.7423][Max branch length: Interaction: F (2, 12) = 0.3205, p=0.7318; Timepoint: F (2, 12) = 2.398, p=0.1330; Group: F (1, 12) = 0.2729, p=0.6109][Num branch points: Interaction: F (2, 12) = 0.1286, p=0.8805; Timepoint: F (2, 12) = 4.621, p=0.0325; Group: F (1, 12) = 0.4333, p=0.5228])(Supp. Figure 5K-N). Overall, Gq manipulation of CaMKII+ neurons did not have an effect on microglial morphology, only aging had an impact.

For GFAP-hM3Dq and mCherry groups, there was a significant interaction between group and time point for microglial cell territory volume (Two-way ANOVA; Interaction: F (2, 12) = 8.377, p=0.0053; Timepoint: F (2, 12) = 5.679, p=0.0184; Group: F (1, 12) = 0.4626, p=0.5093)(Figure 7D). Further analysis revealed that there were pairwise differences between the 3 vs. 6 month GFAP-hM3Dq and mCherry (Tukey's: p=0.0258), and 3 vs. 9 month GFAP-hM3Dq and mCherry groups (Tukey's: p=0.0085), suggesting that our manipulation and aging impacted morphological changes (Figure 7D). For microglial cell volume, there was only an effect of aging (Two-way ANOVA; Interaction: F (2, 12) = 2.353, p=0.1373; Timepoint: F (2, 12) = 5.674, p=0.0184; Group: F (1, 12) = 0.2007, p=0.6622)(Figure 7E). Further, there was a significant interaction between time point and group for microglial ramification index, suggesting that both aging and our manipulation impacted morphological change (Two-way ANOVA; Interaction: F (2, 12) = 4.650, p=0.0320; Timepoint: F (2, 12) = 1.401, p=0.2838; Group: F (1, 12) = 1.751, p=0.2104)(Figure 7F). For average branch length, there was no significant interaction between time point and group (Two-way ANOVA; Interaction: F (2, 12) = 0.8177, p=0.4646; Timepoint: F (2, 12) = 2.600, p=0.1154; Group: F (1, 12) = 0.01994, p=0.8901)(Figure 7G). Additionally, there was no interaction between time point and group for the number of endpoints, minimum branch length, maximum branch length or number of branch points of microglia in the GFAP-hM3Dq and mCherry groups. There was only individual effects of time point for the minimum branch length (Two-way ANOVA; [Num endpoints: Interaction: F (2, 12) = 1.727, =0.2192; Timepoint: F (2, 12) = 1.292, p=0.3104; Group: F (1, 12) = 1.370, p=0.2645][Min branch length: Interaction: F (2, 12) = 1.935, p=0.1869; Timepoint: F (2, 12) = 0.04348, p=0.9576; Group: F (1, 12) = 1.729, p=0.2131][Max branch length: Interaction: F (2, 12) = 1.221, p=0.3291; Timepoint: F (2, 12) = 1.646, p=0.2335; Group: F (1, 12) = 0.1075, p=0.7487][Num branch points: Interaction: F (2, 12) = 1.645, p=0.2337; Timepoint: F (2, 12) = 1.192,

p=0.3372; Group: F (1, 12) = 1.279, p=0.2801])(Supp. Figure 5O-R). Overall, Gq manipulation of GFAP-Gq induced changes in microglial morphology that interacted with normal aging.

3.10) Gq activation of GFAP+ or CaMKII+ cells in vHPC did not affect astrocytic morphology.

To further analyze the impact of our CaMKII or GFAP Gq pathway activation on glial cells, we performed morphological analysis of astrocytes in vHPC. For CaMKII-hM3Dq and mCherry groups, there were no significant interactions between time point and group for astrocytic cell territory volume, total cell volume, ramification index, or average branch length (Two-way ANOVA; [Cell territory volume: Interaction: F (2, 12) = 0.1182, p=0.8896; Timepoint: F (2, 12) = 1.284, p=0.3125; Group: F (1, 12) = 1.850, p=0.1988][Cell volume: Interaction: F (2, 12) = 0.08956, p=0.9149; Timepoint: F (2, 12) = 2.126, p=0.1620; Group: F (1, 12) = 1.509, p=0.2428][Ramification index: Interaction: F (2, 12) = 0.1898, p=0.8296; Timepoint: F (2, 12) = 0.7775, p=0.4814; Group: F (1, 12) = 0.7513, p=0.4031][Avg branch length: Interaction: F (2, 12) = 0.08352, p=0.9204; Timepoint: F (2, 12) = 1.079, p=0.3707; Group: F (1, 12) = 0.6983, p=0.4197])(Figure 6K-N). Additionally, there was no interaction between time point and group for the number of endpoints, minimum branch length, maximum branch length or number of branch points for astrocytes in the CaMKII-hM3Dq and mCherry groups (Two-way ANOVA; [Num endpoints: Interaction: F (2, 12) = 0.4327, p=0.6585; Timepoint: F (2, 12) = 2.567, p=0.1180; Group: F (1, 12) = 1.718, p=0.2145][Min branch length: Interaction: F (2, 12) = 2.461, p=0.1272; Timepoint: F (2, 12) = 1.165, p=0.3449; Group: F (1, 12) = 0.03104, p=0.8631][Max branch length: Interaction: F (2, 12) = 0.1497, p=0.8626; Timepoint: F (2, 12) = 0.8872, p=0.4372; Group: F (1, 12) = 1.199, p=0.2950][Num branch points: Interaction: F (2, 12) = 0.4348, p=0.6572; Timepoint: F (2, 12) = 2.356, p=0.1370; Group: F (1, 12) = 1.539, p=0.2385])(Supp. Figure 6K-N). Interestingly, there was an effect of group for minimum branch length, suggesting that our manipulation of the neuronal Gq pathway was affecting this characteristic of microglia independent of time point for this metric. Overall, Gq activation in CaMKII neurons only affects astrocytic minimum branch length, and no other metrics related to morphological changes.

For GFAP-hM3Dq and mCherry groups, there were no significant interactions between time point and group for astrocytic cell territory volume, total cell volume, ramification index, or average branch length. However, there was an effect of time point alone for both ramification index and average branch length, suggesting an impact of normal aging, but no effect of our Gq manipulation (Two-way ANOVA; [Cell territory volume: Interaction: F (2, 12) = 0.2921, p=0.7519; Timepoint: F (2, 12) = 3.777, p=0.0534; Group: F (1, 12) = 0.1344, p=0.7202][Cell volume: Interaction: F (2, 12) = 0.3062, p=0.7418; Timepoint: F (2, 12) = 1.796, p=0.2079; Group: F (1, 12) = 0.07025, p=0.7955][Ramification index: Interaction: F (2, 12) = 0.05066, p=0.9508; Timepoint: F (2, 12) = 6.080, p=0.0150; Group: F (1, 12) = 0.1177, p=0.7375][Avg branch length: Interaction: F (2, 12) = 2.351, p=0.1375; Timepoint: F (2, 12) = 9.220, p=0.0038; Group: F (1, 12) = 0.01233, p=0.9134])(Figure 7K-N). Additionally, there were no interactions between time point and group for the number of endpoints, minimum branch length, maximum branch length or the number of branch points for astrocytes in the GFAP-hM3Dq and mCherry groups (Two-way ANOVA; [Num endpoints: Interaction: F (2, 12) = 0.7147, p=0.5091; Timepoint: F (2, 12) = 4.391, p=0.0371; Group: F (1, 12) = 0.009931, p=0.9223][Min branch length: Interaction: F (2, 12) = 3.833, p=0.0516; Timepoint: F (2, 12) = 2.432, p=0.1298; Group: F (1,

12) = 0.1621, p=0.6943][Max branch length: Interaction: F (2, 12) = 1.563, p=0.2493; Timepoint: F (2, 12) = 7.779, p=0.0068; Group: F (1, 12) = 0.04654, p=0.8328][Num branchpoints: Interaction: F (2, 12) = 0.5939, p=0.5676; Timepoint: F (2, 12) = 4.401, p=0.0369; Group: F (1, 12) = 0.02290, p=0.8822])(Supp. Figure 6O-R). Overall, Gq activation of the GFAP-Gq pathway does not affect any metrics of astrocytic morphological change, only aging has an impact.

3.11) pTau protein increases at early time points with manipulation of the Gq pathway in neurons and astrocytes, but restores over time.

Neurofibrillary tangles (NFTs) are a pathological hallmark of diseased brain states such as AD and TBI (Castellani & Perry, 2019). NFTs are composed of the microtubule protein known as Tau, which, when phosphorylated (pTau), leads to intracellular aggregations (Braak and Braak, 1991; Bennett et. al., 2006). In-vivo and in- vitro studies have shown that neuronal hyperexcitability significantly increases tau release by neurons (Mohamed et al., 2017; Wu et al., 2016) in models of AD. Additionally, clinical studies have shown that cerebral spinal fluid pTau levels were associated with increased activity in the HPC and age-related cognitive decline (Berron et. al., 2019). To understand how our chronic manipulation of neurons or astrocytes may be inducing an abnormal brain-state, we quantified the presence of Ser202, Thr205 pTau in the vCA1 region of the HPC. This specific isoform for tau is highly upregulated in AD, where it promotes tau mislocalization, aggregation, and leads to the development of NFTs (Neddens et al., 2018; Neddens et al., 2020; Xia et al., 2020). For CaMKII-hM3Dq and mCherry groups, there was a significant interaction between time point and group, indicating that our manipulation of the Gq pathway and age contributed to the presence of pTau (Two-way ANOVA; Interaction: F (2, 12) = 48.08, p<0.0001; Timepoint: F (2, 12) = 48.08, p<0.0001; Group: F (1, 12) = 48.08, p<0.0001)(Figure 8E). *Post hoc* analysis revealed that there was a significant increase in levels of pTau in vCA1 at the 3 month time point (Tukey's: p<0.0001), but not at the 6 or 9 month time points (Figure 8A-B, E). Additionally, we observe a significant difference between 3 vs. 6 month CaMKII-hM3Dq (Tukey's: p<0.0001) and 3 vs. 9 month CaMKII-hM3Dq groups (Tukey's: p<0.0001)(Figure 8E). For GFAP-hM3Dq and mCherry groups, we observe the same interaction between time point and group for pTau levels (Two-way ANOVA; Interaction: F (2, 12) = 46.29, p<0.0001; Timepoint: F (2, 12) = 46.29, p<0.0001; Group: F (1, 12) = 46.29, p<0.0001)(Figure 8F). Additionally, further analysis revealed a similar pattern of pairwise differences between GFAP-hM3Dq and mCherry groups at the 3 month time point, with an increase in pTau in the experimental group (Tukey's: p<0.0001)(Figure 8C-D, F). We also observe the same decrease in pTau between 3 vs. 6 month GFAP-hM3Dq (Tukey's: p<0.0001) and 3 vs. 9 month GFAP-hM3Dq groups (Tukey's: p<0.0001)(Figure 8F). Together, this suggests that our chronic Gq manipulation is facilitating the expression of hyperphosphorylated tau in the HPC at early time points. We speculate that as the Gq modulation progresses, the brain adapts by clearing pTau expression and returns to a baseline state of homeostasis. Future research can investigate the causal molecular pathways that become activated to promote and suppress the expression of pTau and to thereby investigate possible targets for future disease modulation.

4) Discussion.

Our findings demonstrate that chronic activation of the Gq pathway in neurons and astrocytes differentially affects fear memory and anxiety-related behaviors, as well as markers of cellular stress. Notably, these manipulations did not significantly affect many aspects of social interaction, spatial odor memory, y-maze navigation behaviors, nor glial number of morphology compared to controls. Together, our results add to burgeoning literature demonstrating that chemogenetic, optogenetic and pharmacological manipulation of neurons and astrocytes across numerous brain regions induces behavioral enhancement or impairment, including in memory, anxiety, attention, locomotion and feeding (Nagai et. al., 2019; Chen et. al., 2016; Adamsky et. al., 2018; Martin-Fernandez et. al., 2017; Xiao et. al., 2020; Lei et. al., 2022; Shelkar et. al., 2021; Li et. al., 2020; Padilla-Coreano et. al., 2017; Deisseroth et. al., 2014; Jimenez et. al., 2018; Jennings et. al., 2013; Stuber et. al., 2012). Although these studies begin to address the role of these cell types in a variety of behaviors, there is a gap in our understanding of what prolonged or "chronic" manipulations do to network functioning as it relates to behavioral output. Our study aims to address both of these gaps with chronic manipulation of the Gq pathway within vCA1.

Notably, recent work has addressed the importance of the differences in how astrocytes and neurons respond to external perturbation. For instance, Gi- and Gq-activation in astrocytes stimulates the release of extracellular glutamate and increases neuronal excitability, suggesting that inhibitory signaling may be a unique property to neurons (Durkee et. al., 2019). Another study has shown that Gq- and Gi-pathways in astrocytes drive synaptic potentiation in hippocampal CA1 via Ca^{2+}-dependent and Ca^{2+}-independent mechanisms, respectively (Van Den Herrewegen et. al., 2021). This suggests that our astrocytic Gq manipulation strategy may be inducing unique cellular outcomes compared to neuronal Gq activation, and future studies can seek to tease out the differential mechanisms underlying each.

Our study provides evidence that cell-type specific targeting induces differential effects on behavioral outcome, which may help inform subsequent treatments for disorders of the brain. For instance, while deep brain stimulation (DBS) and transcranial magnetic stimulation (TMS) are often effective in the treatment of psychiatric disorders, the cell-types directly affected through each perturbation and their outcomes remain ripe for exploration. Along similar lines, recent literature has suggested that clinical DBS-like, high-frequency stimulation of human astrocytes promotes changes in gene expression that are relevant to extracellular matrix formation, likely aiding in synapse development and induction of neuronal plasticity (Jang et. al., 2019). Further understanding of how these techniques may be non-discriminately targeting all cells within a brain region vs. specific cell-types to exert their effects on network functioning and improvement in symptomatology would improve their efficacy. Our work suggests that targeting astrocytes or neurons within the vHPC may be an effective means to differentially modulate fear, anxiety, and social behaviors.

Finally, chronic manipulation of Gq pathways in neurons and astrocytes across time has inherent limitations. DREADD-mediated cell activation has not been as thoroughly investigated with chronic use, as it has been in acute administration studies. As such, it is possible that across 9 months, the efficacy of the ligand binding decreases over time. However, and promisingly, we observe persistence in the receptor expression, as indicated by the robust expression of hM3Dq-mCherry across 3, 6 and 9 month time points in both cell types,

suggesting its existing functionality. Additionally, we see significant impact on behavior at the latest time point in both neuronal and astrocytic groups. Indeed, even if the DREADD-mediated manipulation was only robust until the 3 month time point, we are still inducing pronounced network insults and increasing cellular markers of stress (pTau) that have persistent effects on behavior later in time.

Future research may investigate the *in vivo* physiological response using electrophysiology in vCA1 across time points as these cells are chronically activated. The impact of this would be two-fold: understanding how cellular activity changes of neurons in vCA1 change with manipulation across time, and confirming physiological response of these cells to the manipulation with a more concrete read-out than behavior. This would additionally allow for investigation of how cellular activity is related to the different behavioral changes (e.g. early changes in anxiety-related behaviors vs. later changes in fear memory), as well as the 'recovery' from pTau expression at the 6 and 9 month time points. We speculate that the brain's excitatory-inhibitory balance is undergoing homeostatic changes with time and especially with chronic manipulation, therefore leading to the clearance of pTau cellular aggregates.

Overall, our data suggests that chronic manipulation of the Gq pathway in neurons and astrocytes across multiple time points impacts fear memory and anxiety-related behaviors. This information provides valuable insights into the differential effects of chemogenetic manipulations of multiple cell types in a single brain region, as well as the specific effects of network disruption in the vHPC on cellular and behavioral phenotypes.

Data Availability Statement

The data that support the findings of this study are available from the corresponding author upon reasonable request.

Acknowledgements

This work was supported by a Ludwig Family Foundation grant, an NIH Early Independence Award (DP5 OD023106-01), an NIH Transformative R01 Award, a Young Investigator Grant from the Brain and Behavior Research Foundation, the McKnight Foundation Memory and Cognitive Disorders award, the Pew Scholars Program in the Biomedical Sciences, the Air Force Office of Scientific Research (FA9550-21-1-0310), the Center for Systems Neuroscience and Neurophotonics Center at Boston University.

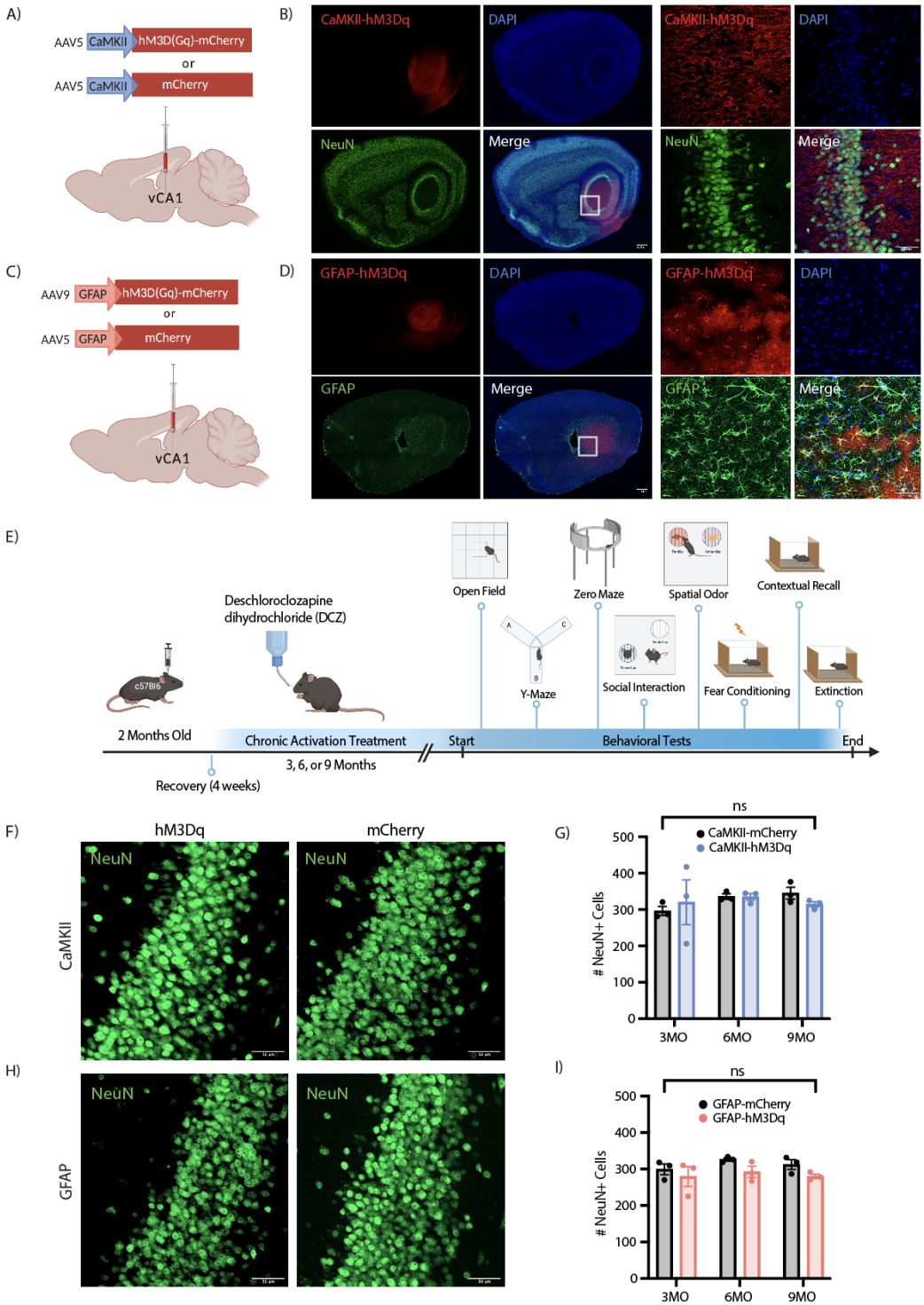

Figure 1. Chronic activation of Gq pathways in CaMKII+ neurons and GFAP+ astrocytes in vCA1. (A) Viral strategy schematic for the neuronal groups. The AAV5-CaMKII-hM3D(Gq)-mCherry or control vector AAV5-CaMKII-mCherry was bilaterally injected into the vCA1 region of wild type mice. (B) Representative images of RFP/NeuN+ co-staining (red and green, respectively) and DAPI+ cells (blue). (C) Viral strategy schematic for the astrocyte groups. The AAV9-GFAP-hM3D(Gq)-mCherry or control vector AAV5-GFAP-mCherry was bilaterally injected into the vCA1 region of wild type mice. (D) Representative images of RFP/GFAP+ co-staining (red and green, respectively) and DAPI+ cells (blue). (E) Schematic representation of chronically activating neuron or astrocyte Gq receptors through administration of the water-soluble DREADD ligand deschloroclozapine dihydrochloride (DCZ) for either 3, 6, or 9 months. Mice underwent a battery of behavior at each end point. (F-I) Histological assessment of NeuN+ cells to determine whether our manipulations were killing vCA1 neurons in the CaMKII groups (F and G) and/or GFAP groups (H and J). NeuN counts were assessed with a two-way analysis of variance (ANOVA) with time point and group as factors. Error bars indicate SEM. $p \leq 0.05$, $^{**}p \leq 0.01$, $^{***}p \leq 0.001$, $^{****}p \leq 0.0001$, ns = not significant. Per group: n= 3 mice x 18 tiles (region of interest (ROI): vCA1) each were quantified for statistical analysis of NeuN counts.

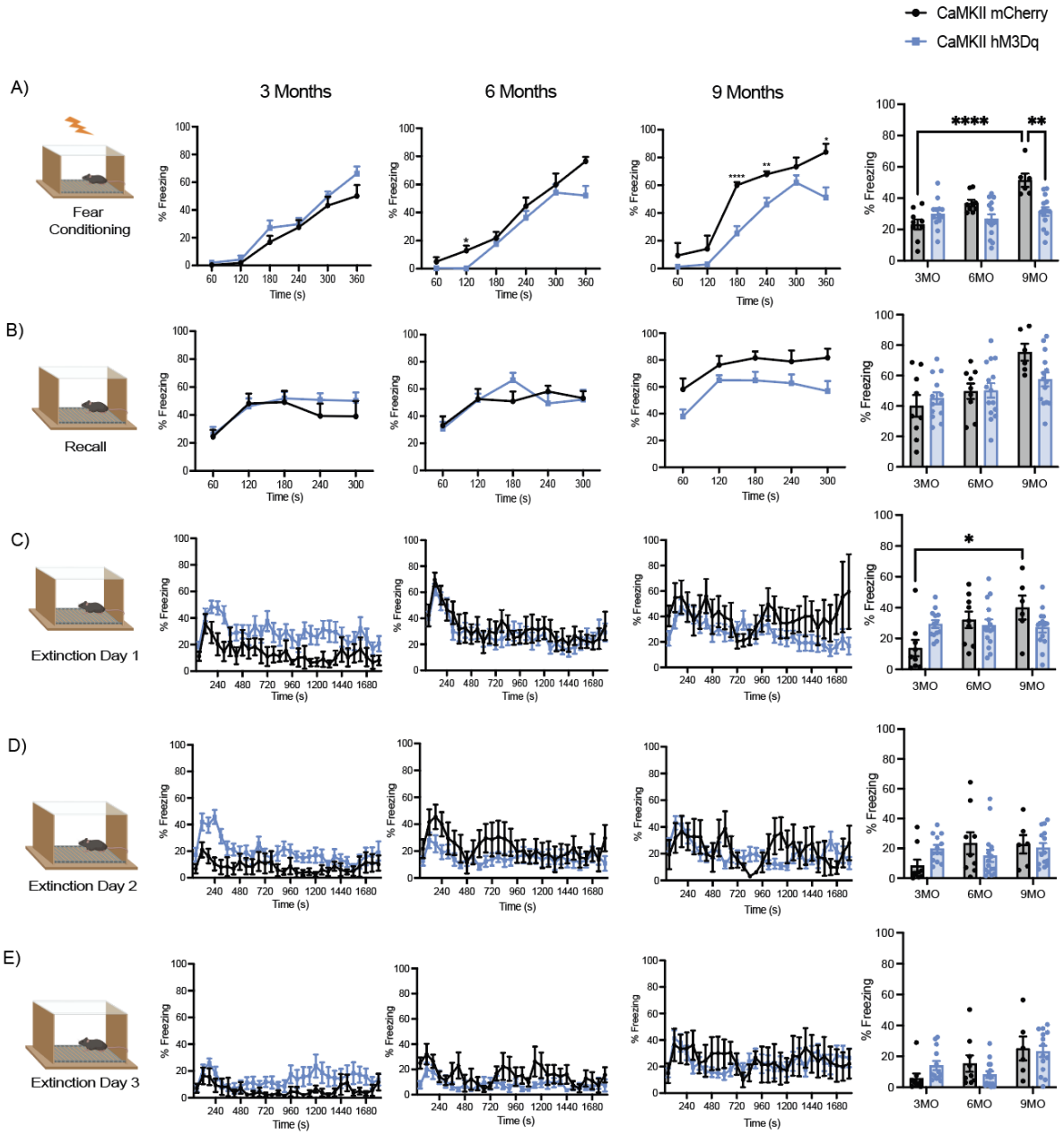

Figure 2. Chronic Gq activation of CaMKII+ neurons induces behavioral changes in contextual fear acquisition and maintenance. (A-E) Percent freezing levels and freezing percentage across time (seconds) of 3, 6, and 9 month time points. (A) CaMKII groups during contextual fear conditioning (CFC), where mice received four, 1.5mA foot shocks at 120, 180, 240 and 300 seconds during a 360 second session, (B) recall session for 360 seconds, where mice did not receive the aversive stimulus, (C) extinction day 1, (D) day 2 and (E) day 3, where mice received no foot shock for 900 second sessions. Average percent freezing was assessed with a two-way analysis of variance (ANOVA) with time point and group as factors. Freezing percentage across the 1-minute time bins [60, 120, 180, 240, 300, 360] was assessed with a two-way ANOVA with repeated measures (RM) with

time (seconds) and group as factors. Tukey's and Sidak's *post hoc* tests were performed where applicable. Error bars indicate SEM. $p \leq 0.05$, $^{**}p \leq 0.01$, $^{***}p \leq 0.001$, $^{****}p \leq 0.0001$, ns = not significant. 3 Month: hM3Dq (n=13), mCherry (n=9); 6 Month: hM3Dq (n=15), mCherry (n=9); 9 Month: hM3Dq (n=14), mCherry (n=6).

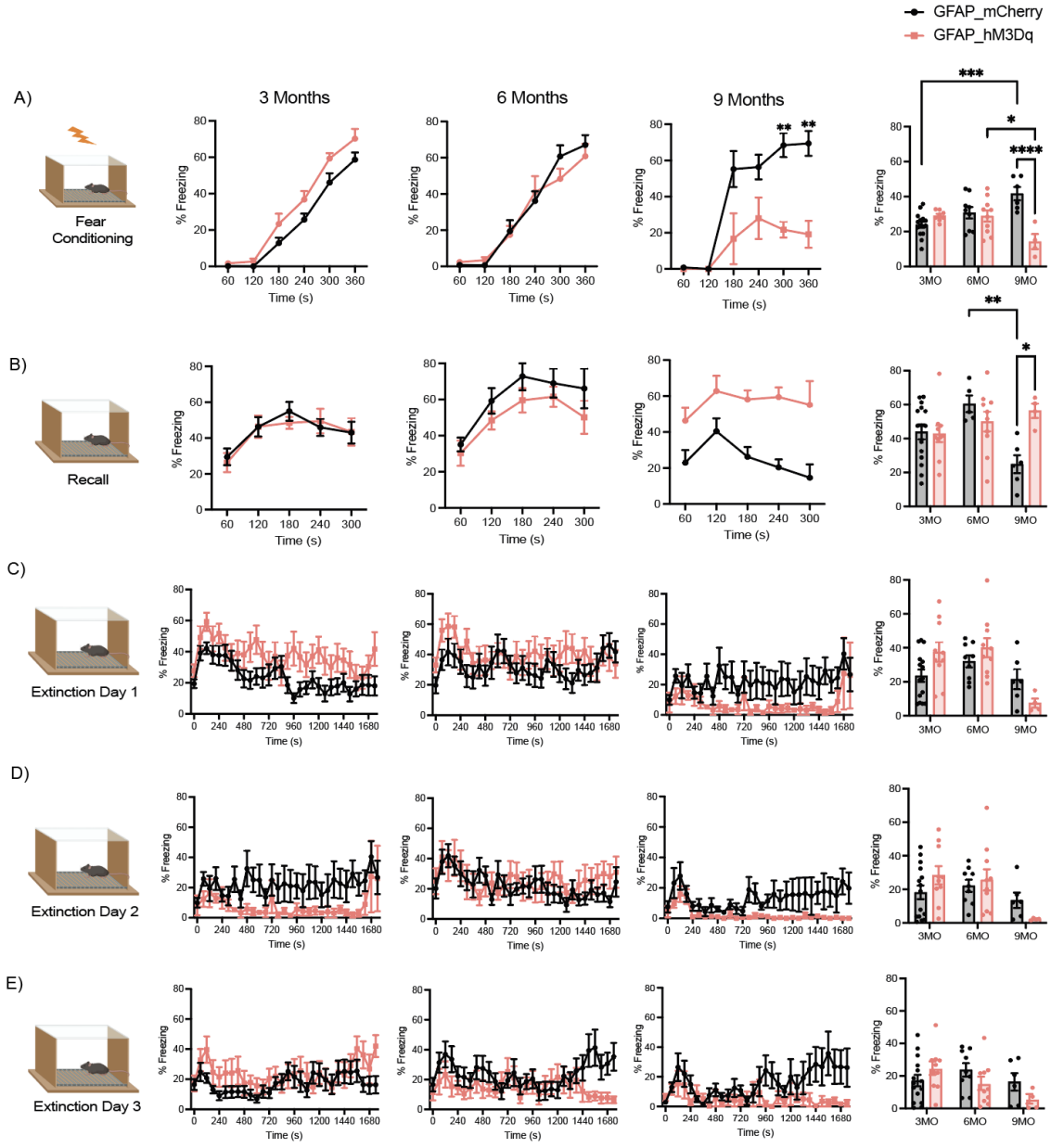

Figure 3. Gq pathway activation in GFAP+ astrocytes impairs acquisition and enhances recall of contextual fear memory at the 9 month time point. (A-E) Percent freezing levels and freezing percentage across time (seconds) of 3, 6, and 9 month time points. (A) GFAP groups during contextual fear conditioning (CFC), where mice received four, 1.5mA foot shocks at 120, 180, 240 and 300 seconds during a 360 second session,(B) recall session for 360 seconds, where mice did not receive the aversive stimulus, (C) extinction day 1,

(D) day 2, and (E) day 3, where mice received no foot shock for a 900 second session. Average percent freezing was assessed with a two-way analysis of variance (ANOVA) with time point and group as factors. Freezing percentage across the 1-minute time bins [60, 120, 180, 240, 300, 360] was assessed with a two-way ANOVA with repeated measures (RM) with time (seconds) and group as factors. Tukey's and Sidak's *post hoc* tests were performed where applicable. Error bars indicate SEM. $p \leq 0.05$, $^{**}p \leq 0.01$, $^{***}p \leq 0.001$, $^{****}p \leq 0.0001$, ns = not significant. 3 Month: hM3Dq (n=10), mCherry (n=15); 6 Month: hM3Dq (n=10), mCherry (n=5-9); 9 Months: hM3Dq (n=4), mCherry (n=9).

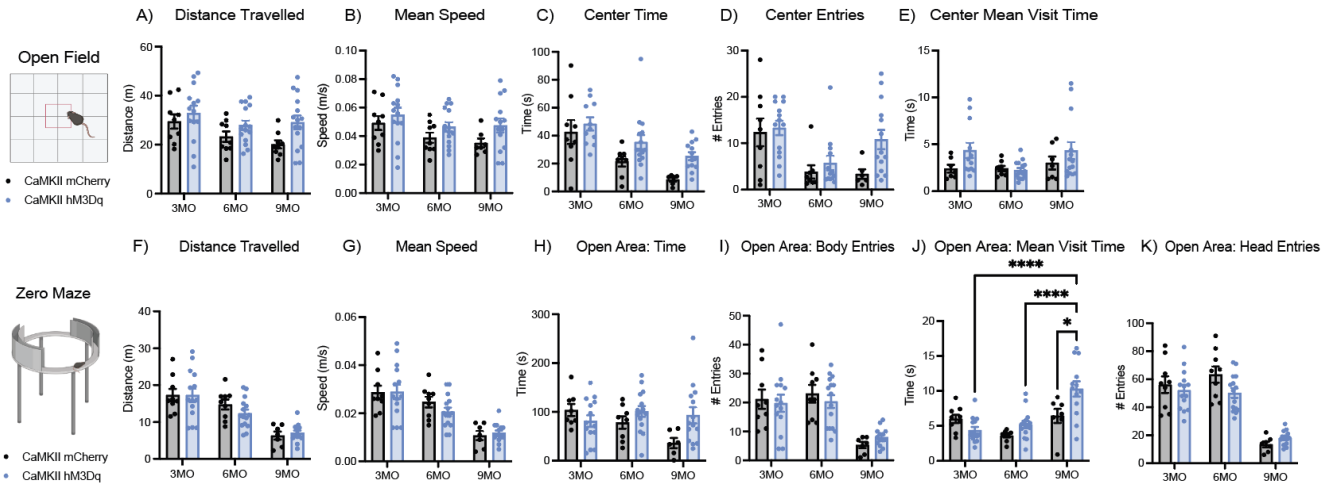

Figure 4. Chronic Gq activation of neurons induces behavioral changes in locomotor and anxiety-related behaviors. (A-E) Open field distance traveled (A), mean speed (B), total time spent in center (C), number of entries into center (D), and mean center visit time (E) in 3, 6, and 9 month CaMKII groups. (F-M) Zero maze distance traveled (F), mean speed (G), total time spent in open area (H), number body entries into open area (I), mean open area visit time (J), and number of head entries into open area (K) in 3, 6, and 9 month CaMKII groups. Open field and zero maze metrics were assessed with a two-way analysis of variance (ANOVA) with time point and group as factors. Tukey's *post hoc* tests were performed where applicable. Error bars indicate SEM. $p \leq 0.05$, $^{**}p \leq 0.01$, $^{***}p \leq 0.001$, $^{****}p \leq 0.0001$, ns = not significant. For open field, 3 Month: hM3Dq (n=11-14), mCherry (n=7-9); 6 Months: hM3Dq (n=13-15), mCherry (n=8-9); 9 Months: hM3Dq (n=12-15), mCherry (n=6-9) after outlier removal. For zero maze, 3 Month: hM3Dq (n=14), mCherry (n=9); 6 Month: hM3Dq (n=15), mCherry (n=8-9); 9 Month: hM3Dq (n=14), mCherry (n=6-7) after outlier removal.

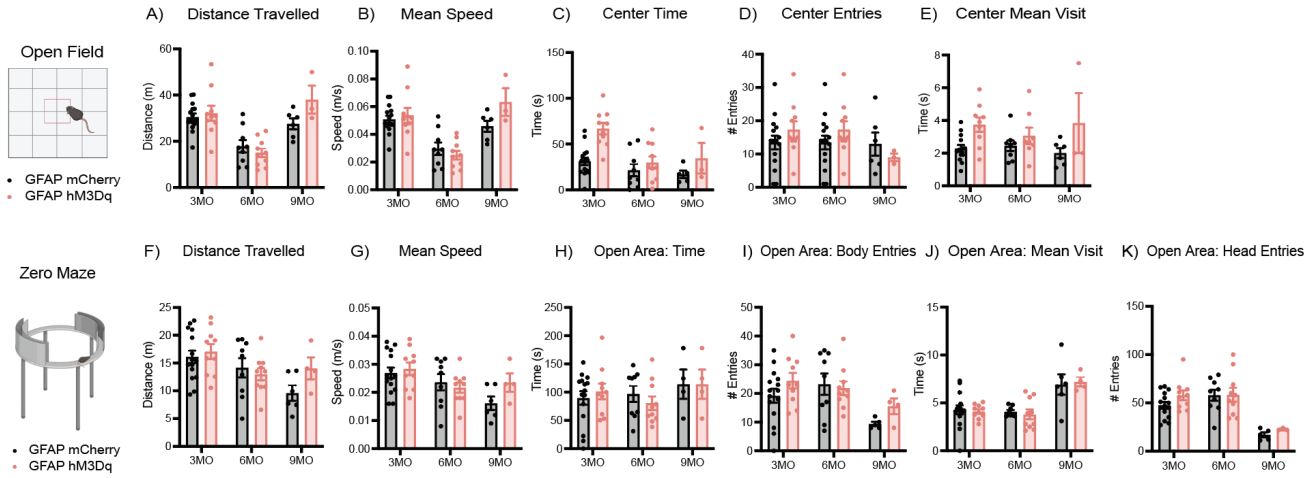

Figure 5. Chronic Gq activation of astrocytes induces behavioral changes in locomotor and anxiety-related behaviors. (A-E) Open field distance traveled (A), mean speed (B), total time spent in center (C), number of entries into center (D), and mean center visit time (E) in 3, 6, and 9 month GFAP groups. (F-M) Zero maze distance traveled (F), mean speed (G), total time spent in open area (H), number body entries into open area (I), mean open area visit time (J), and number of head entries into open area (K) in 3, 6, and 9 month GFAP groups. Open field and zero maze metrics were assessed with a two-way analysis of variance (ANOVA) with time point and group as factors. Tukey's *post hoc* tests were performed where applicable. Error bars indicate SEM. $p \leq 0.05$, $^{**}p \leq 0.01$, $^{***}p \leq 0.001$, $^{****}p \leq 0.0001$, ns = not significant. For open field, 3 Month: hM3Dq (n=10), mCherry (n=15); 6 Month: hM3Dq (n=10), mCherry (n=9-15); 9 Month: hM3Dq (n=3), mCherry (n=6) after outlier removal. For zero maze, 3 Month: hM3Dq (n=10), mCherry (n=15); 6 Month: hM3Dq (n=10), mCherry (n=9); 9 Month: hM3Dq (n=4), mCherry (n=6) after outlier removal.

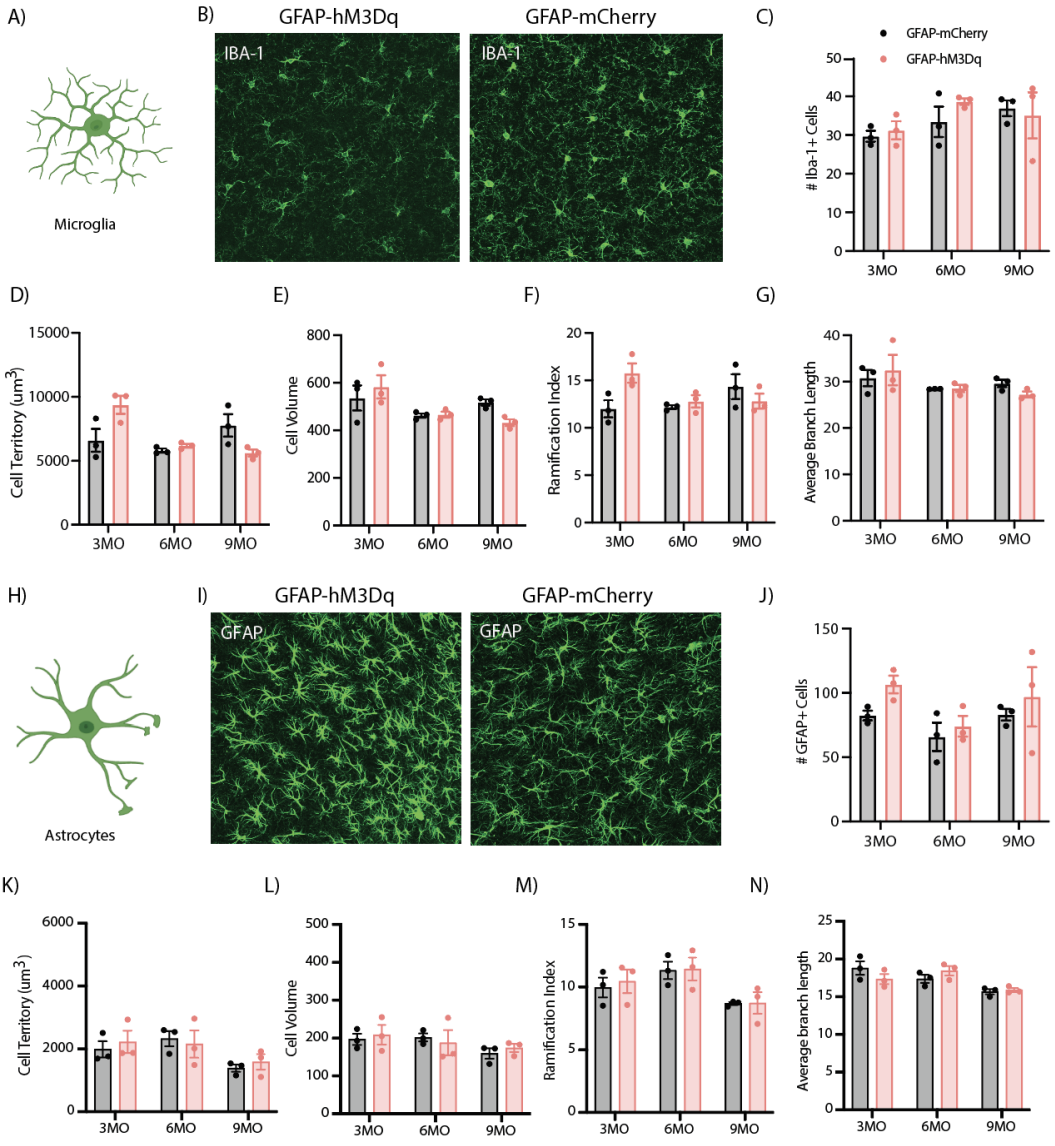

Figure 6. GFAP-hM3Dq activation mildly impacted microglial, but not astrocytic morphology.
(A) Schematic of microglia morphology. (B) Representative single tile images of IBA-1+ cells in CaMKII-hM3Dq and CaMKII-mCherry groups. (C) Number of Iba-1+ cells counted in 3, 6, and 9 month CaMKII groups. (D-G) Quantification of Iba-1+ (D) cell territory volume, (E) cell volume, (F) ramification index, and (G) average branch length in 3, 6, and 9 month CaMKII groups. (H) Schematic of astrocyte morphology. (I) Representative images of GFAP+ cells in CaMKII-hM3Dq and CaMKII-mCherry groups. (J) Number of GFAP+ cells counted in 3, 6, and 9 month CaMKII groups. (K-N) Quantification of GFAP+ (K) cell territory volume, (L) cell volume, (M) ramification index, and (N) average branch length in 3, 6, and 9 month CaMKII groups. Cell count and morphology metrics were assessed with a two-way analysis of variance (ANOVA) with time point and group as factors. Tukey's *post hoc* tests were performed where applicable. Error bars indicate SEM. $p \leq 0.05$, $^{**}p \leq 0.01$, $^{***}p \leq 0.001$, $^{****}p \leq 0.0001$, ns = not significant. All groups: n= 3 mice

x 18 tiles (ROI: vCA1) each were quantified for statistical analysis of astrocytic and microglial morphology per group.

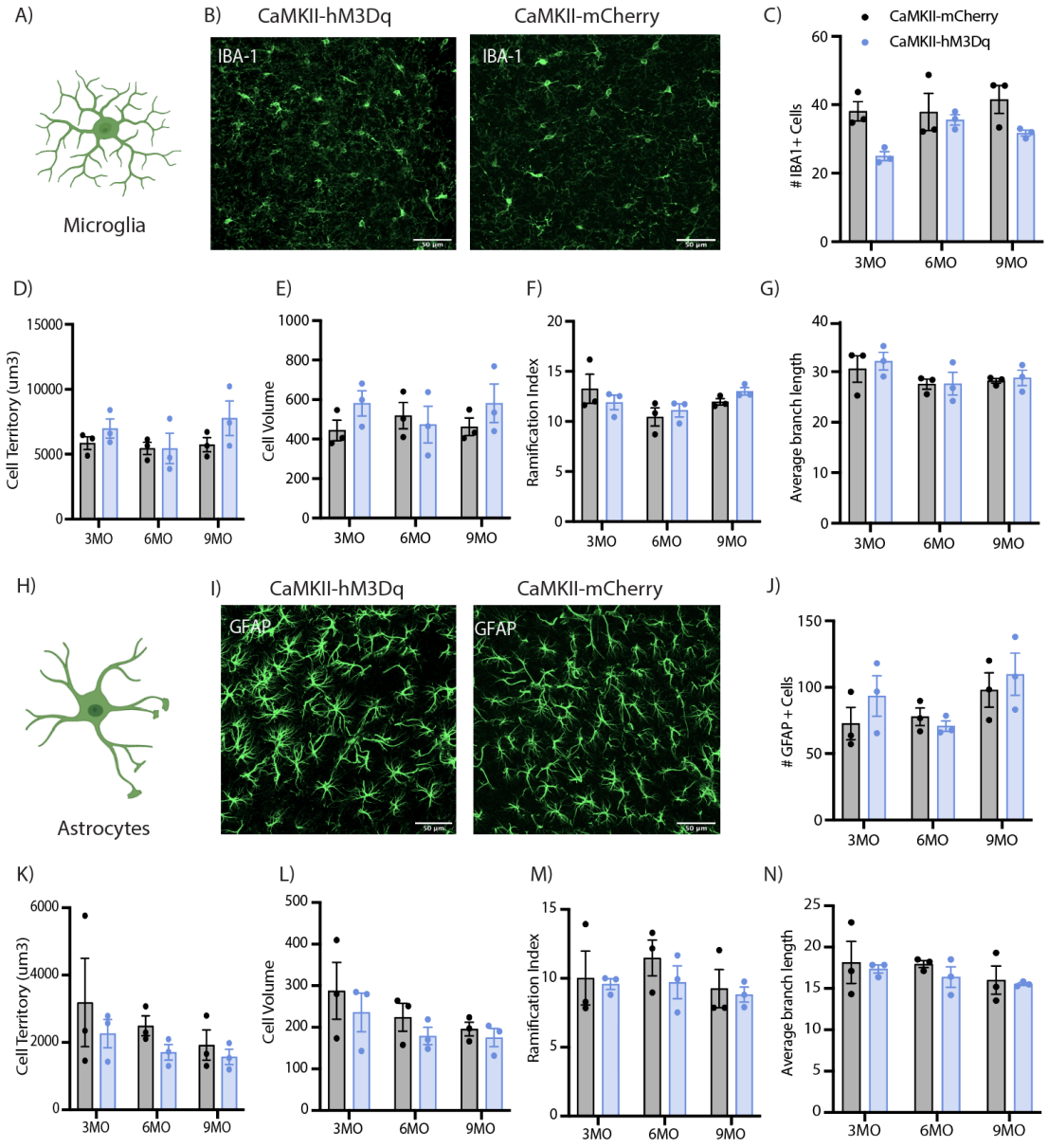

Figure 7. CaMKII-hM3Dq activation mildly impacted microglial and astrocytic morphology. (A) Schematic of microglia morphology. (B) Representative images of Iba-1+ cells in GFAP-hM3Dq and GFAP-mCherry groups. (C) Number of Iba-1+ cells counted in 3, 6, and 9 month GFAP groups. (D-G) Quantification of Iba-1+ (D) cell territory volume, (E) cell volume, (F) ramification index, and (G) average branch length in 3, 6, and 9 month GFAP groups. (H) Schematic of astrocyte morphology. (I) Representative images of GFAP+ cells in GFAP-hM3Dq and GFAP-mCherry groups. (J) Number of GFAP+ cells counted in 3, 6, and 9 month GFAP-hM3Dq and GFAP-mCherry groups. (K-N) Quantification of GFAP+ (K) cell

territory volume, (L) cell volume, (M) ramification index, and (N) average branch length in 3, 6, and 9 month GFAP groups. Cell count and morphology metrics were assessed with a two-way analysis of variance (ANOVA) with time point and group as factors. Tukey's *post hoc* tests were performed where applicable. Error bars indicate SEM. $p \leq 0.05$, $^{**}p \leq 0.01$, $^{***}p \leq 0.001$, $^{****}p \leq 0.0001$, ns = not significant. All groups: n= 3 mice x 18 tiles (ROI: vCA1) each were quantified for statistical analysis of astrocytic and microglial morphology per group.

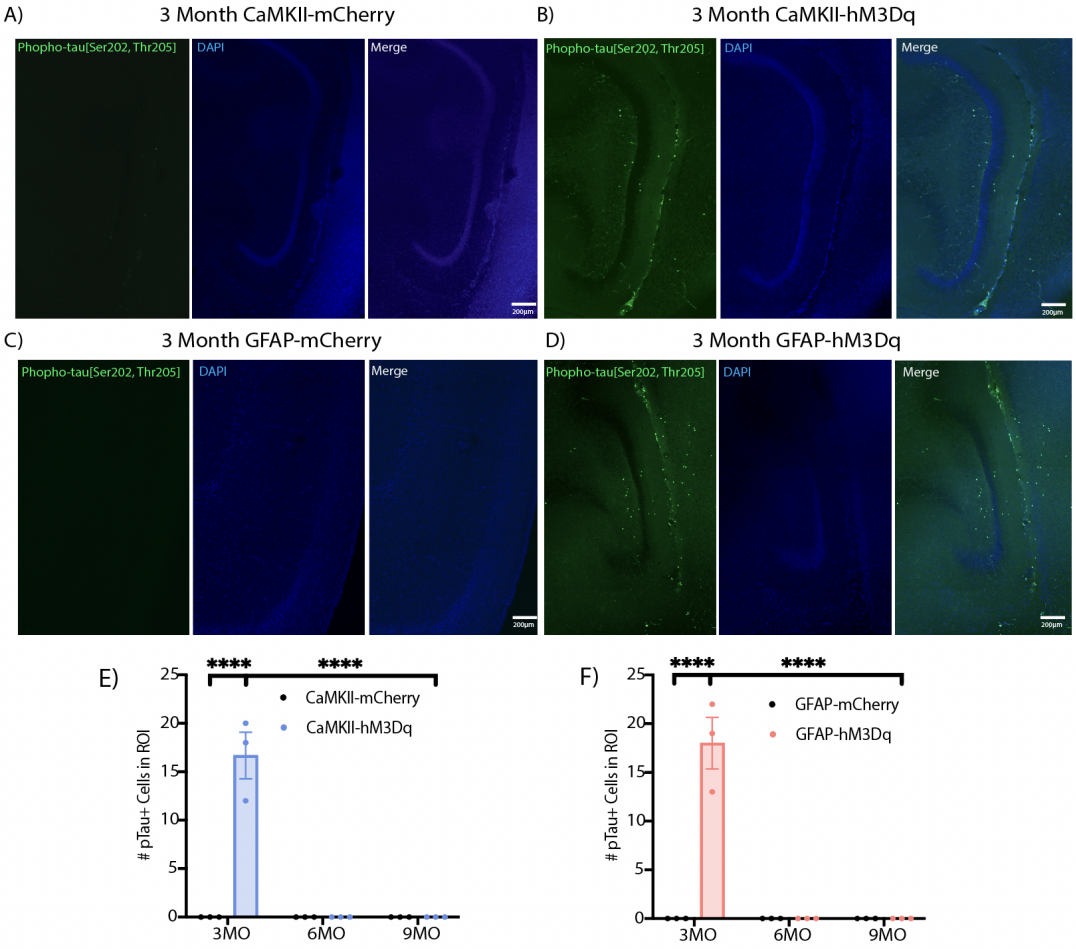

Figure 8: Neurofibrillary tangle protein increases at early time points with manipulation of the Gq pathway in neurons and astrocytes, but restores over time. (A) Representative image of pTau expression in a sagittal section of the hippocampus (HPC)in the 3 Month CaMKII-mCherry group. (B) Representative image of pTau expression in a sagittal section of the HPC in the 3 Month CaMKII-hM3Dq-mCherry group. (C) Representative image of pTau expression in a sagittal section of the HPC in the 3 Month GFAP-mCherry group. (D) Representative image of pTau expression in a sagittal section of the HPCin the 3 Month GFAP-hM3Dq-mCherry group. (E) Number of pTau+ positive cells in designated ROI of the HPC in the CAMKII manipulation group. (F) Number of pTau+ positive cells in designated ROI of the HPC in the GFAP manipulation group. Number of pTau+ cells was assessed with a two-way analysis of variance (ANOVA) with time point and group as factors. Tukey's *post hoc* tests were performed where applicable. Error bars indicate

SEM. $p \leq 0.05$, $^{**}p \leq 0.01$, $^{***}p \leq 0.001$, $^{****}p \leq 0.0001$, ns = not significant. All groups: n= 3 mice x 4 slices (ROI: vCA1) each were quantified for statistical analysis of astrocytic and microglial morphology per group.

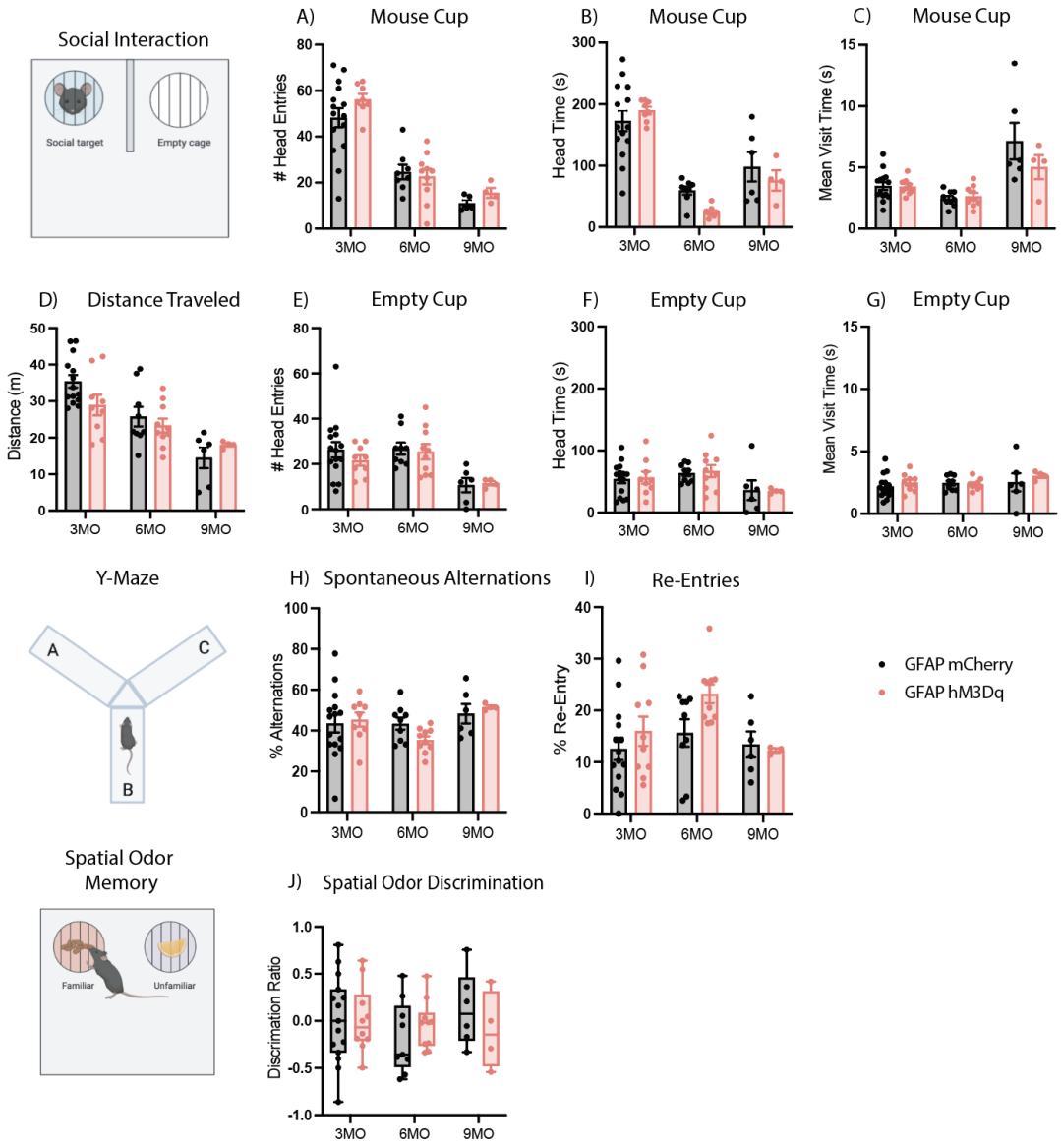

Supplemental Figure 1: Chronic Gq activation of astrocytes in vCA1 does not affect behavior in social interaction, y-maze or spatial odor memory. (A-C) Social interaction mouse cup (e.g. social target) number of head entries (A), head time (B), and mean visit time (C) across the 3, 6 and 9 month GFAP-mCherry and hM3Dq groups. (D) Total distance traveled across the entire testing chamber. (E-G) Social interaction empty cup (i.e. control target) number of head entries (E), head time (F), and mean visit time (G) across the 3, 6 and 9 month GFAP-mCherry and hM3Dq groups. (H-I) Elevated y-maze percentage of spontaneous alternations (e.g. sequence of non-repeating arms; ABC, CBA) (H) and percentage of re-entries into the same arm (e.g. AA, BB,

CC). (J) Spatial odor memory discrimination ratio across all timepoints for GFAP-mCherry and hM3Dq groups. Social interaction, y-maze and spatial odor memory metrics were assessed with a two-way analysis of variance (ANOVA) with time point and group as factors. Tukey's *post hoc* tests were performed where applicable. Error bars indicate SEM. $p \leq 0.05$, $^{**}p \leq 0.01$, $^{***}p \leq 0.001$, $^{****}p \leq 0.0001$, ns = not significant. For social interaction, 3 Month: hM3Dq (n=8-9), mCherry (n=15); 6 Month: hM3Dq (n=10), mCherry (n=8); 9 Month: hM3Dq (n=4), mCherry (n=6) after outlier removal. For spatial odor, 3 Month: hM3Dq (n=10), mCherry (n=15); 6 Month: hM3Dq (n=10); mCherry (n=9); 9 Month: hM3Dq (n=4), mCherry (n=6) after outlier removal. For y-maze, 3 Month: hM3Dq (n=10), mCherry (n=15); 6 Month: hM3Dq (n=10), mCherry (n=9); 9 Month: hM3Dq (n=4), mCherry (n=6) after outlier removal.

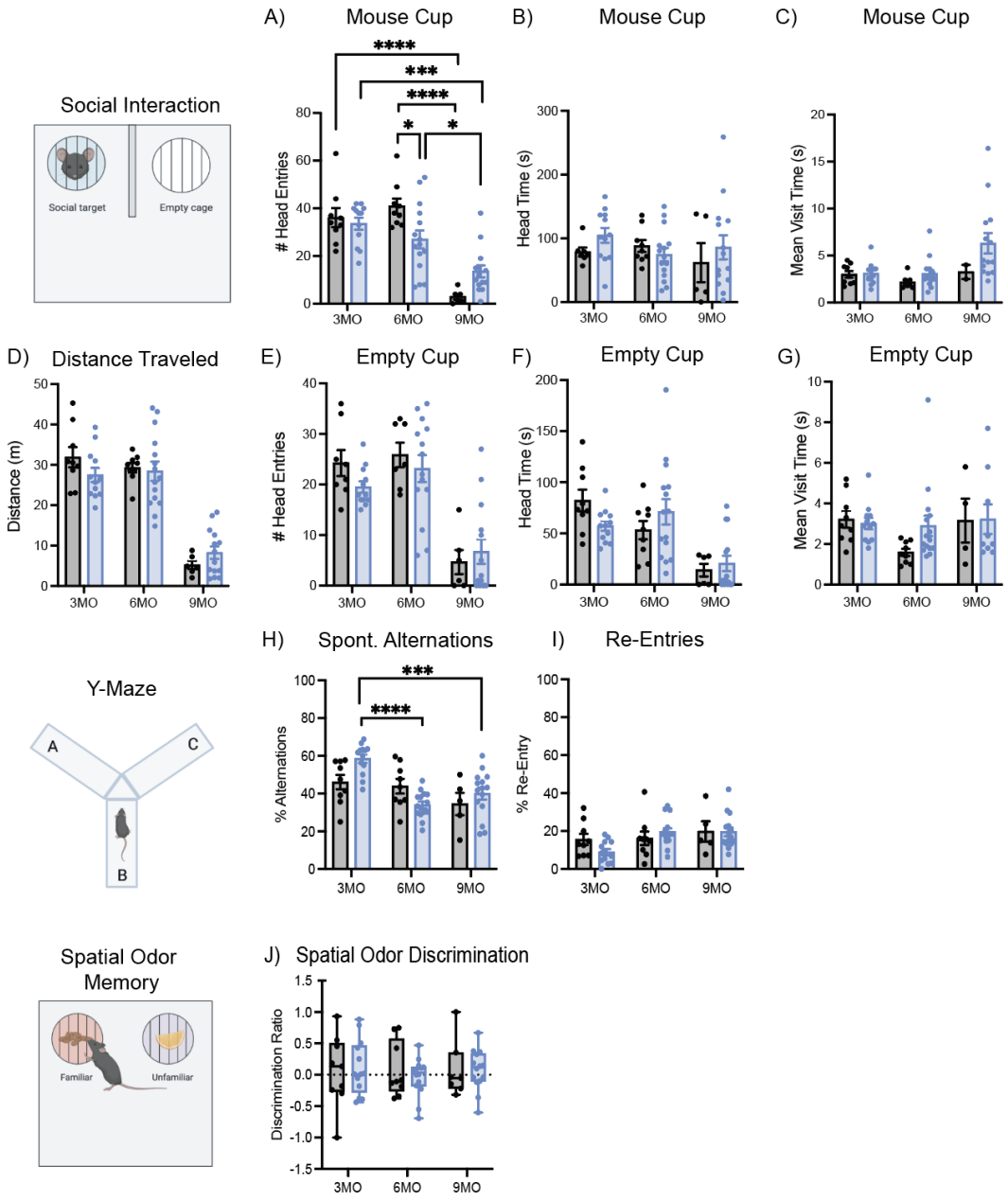

Supplemental Figure 2: Chronic Gq activation of neurons in vCA1 decreases social engagement at the 6 month time point, and impacts y-maze, but not spatial odor memory behavior. (A-C) Social interaction mouse cup (e.g. social target) number of head entries (A), head time (B), and mean visit time (C) across the 3, 6 and 9 month CaMKII-mCherry and hM3Dq groups. (D) Total distance traveled across the entire testing chamber. (E-G) Social interaction empty cup (i.e. control target) number of head entries (E), head time (F), and mean visit time (G) across the 3, 6 and 9 month CaMKII-mCherry and hM3Dq groups. (H-I) Elevated y-maze percentage of spontaneous alternations (e.g. sequence of non-repeating arms; ABC, CBA) (H) and percentage of re-entries into the same arm (e.g. AA, BB, CC). (J) Spatial odor memory discrimination ratio

across all timepoints for CaMKII-mCherry and hM3Dq groups. Social interaction, y-maze and spatial odor memory metrics were assessed with a two-way analysis of variance (ANOVA) with time point and group as factors. Tukey's *post hoc* tests were performed where applicable. Error bars indicate SEM. $p \leq 0.05$, $^{**}p \leq 0.01$, $^{***}p \leq 0.001$, $^{****}p \leq 0.0001$, ns = not significant. For social interaction, 3 Month: hM3Dq (n=12), mCherry (n=9); 6 Month: hM3Dq (n=15), mCherry (n=9); 9 Month: hM3Dq (n=14), mCherry (n=6) after outlier removal. For spatial odor memory, 3 Month: hM3Dq (n=13), mCherry (n=9); 6 Month: hM3Dq (n=15), mCherry (n=9); 9 Month: hM3Dq (n=14), mCherry (n=7) after outlier removal. For y-maze, 3 Month: hM3Dq (n=13), mCherry (n=9); 6 Month: hM3Dq (n=15), mCherry (n=9); 9 Month: hM3Dq (n=15), mCherry (n=5) after outlier removal.

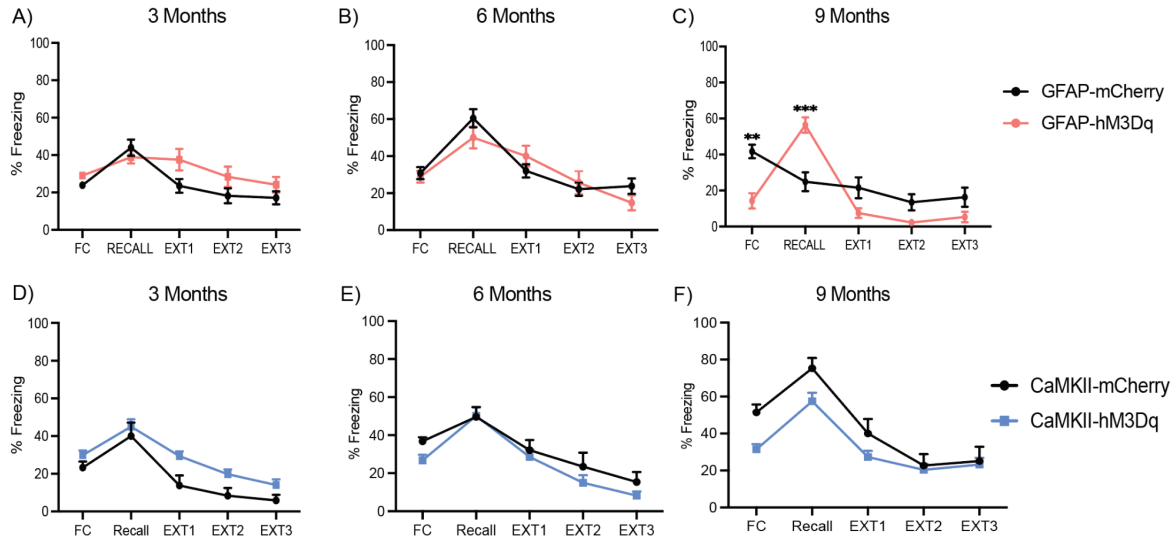

Supplemental Figure 3: Chronic Gq activation of neurons or astrocytes differentially affects acquisition and recall of a contextual fear memory. (A-C) Average percent freezing (%) across fear conditioning, recall, extinction days 1-3 for GFAP-mCherry and hM3Dq groups at the 3 month (A), 6 month (B) and 9 month (C) timepoints. (D-F) Average percent freezing (%) across fear conditioning, recall, extinction days 1-3 for CaMKII-mCherry and hM3Dq groups at the 3 month (A), 6 month (B) and 9 month (C) timepoints. Average freezing percentage across days [FC, Recall, EXT1, EXT2, EXT3] was assessed with a two-way ANOVA with repeated measures (RM) with day and group as factors. Sidak's *post hoc* tests were performed where applicable. Error bars indicate SEM. $p \leq 0.05$, $^{**}p \leq 0.01$, $^{***}p \leq 0.001$, $^{****}p \leq 0.0001$, ns = not significant. For CaMKII groups, 3 Month: hM3Dq (n=13), mCherry (n=9); 6 Month: hM3Dq (n=15), mCherry (n=9); 9 Month: hM3Dq (n=14), mCherry (n=6) after outlier removal. For GFAP groups, 3 Month: hM3Dq (n=10), mCherry (n=15); 6 Month: hM3Dq (n=10), mCherry (n=5-9); 9 Month: hM3Dq (n=4), mCherry (n=6) after outlier removal.

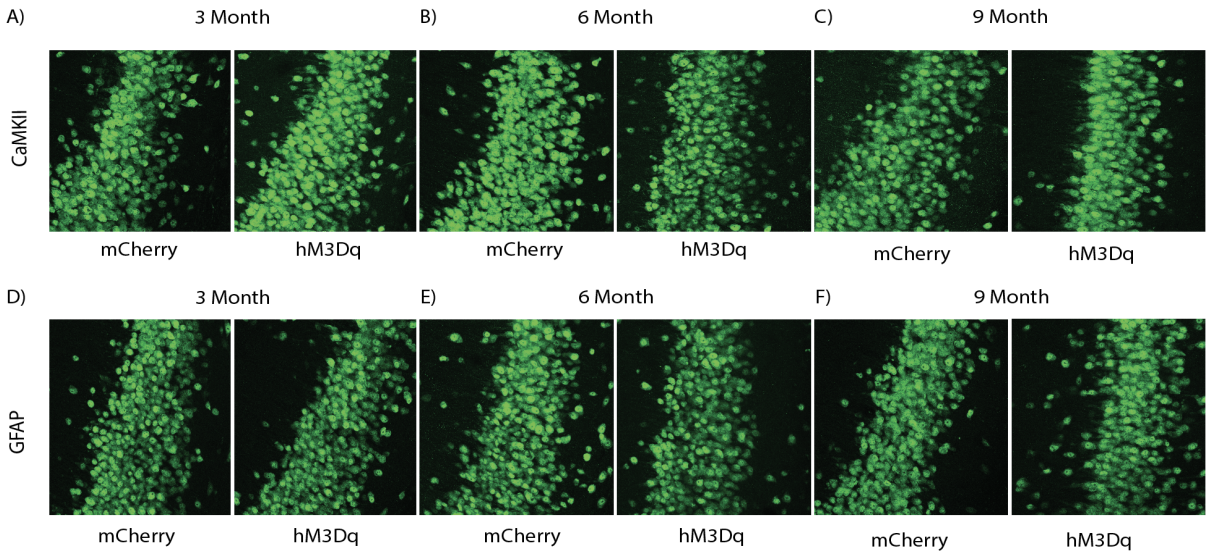

Supplemental Figure 4: Gq pathway activation for 3, 6 or 9 months does not increase cell death in the vCA1 region of the hippocampus in any group or time point. (A-C) Representative hippocampal ventral CA1 NeuN (green) expression for CaMKII-mCherry and hM3Dq groups for the 3 month (A), 6 month (B) and 9 month (C) timepoints to quantify cell loss in the region of manipulation. (D-F) Representative hippocampal ventral CA1 NeuN expression for GFAP-mCherry and hM3Dq groups for the 3 month (D), 6 month (E) and 9 month (F) timepoints.

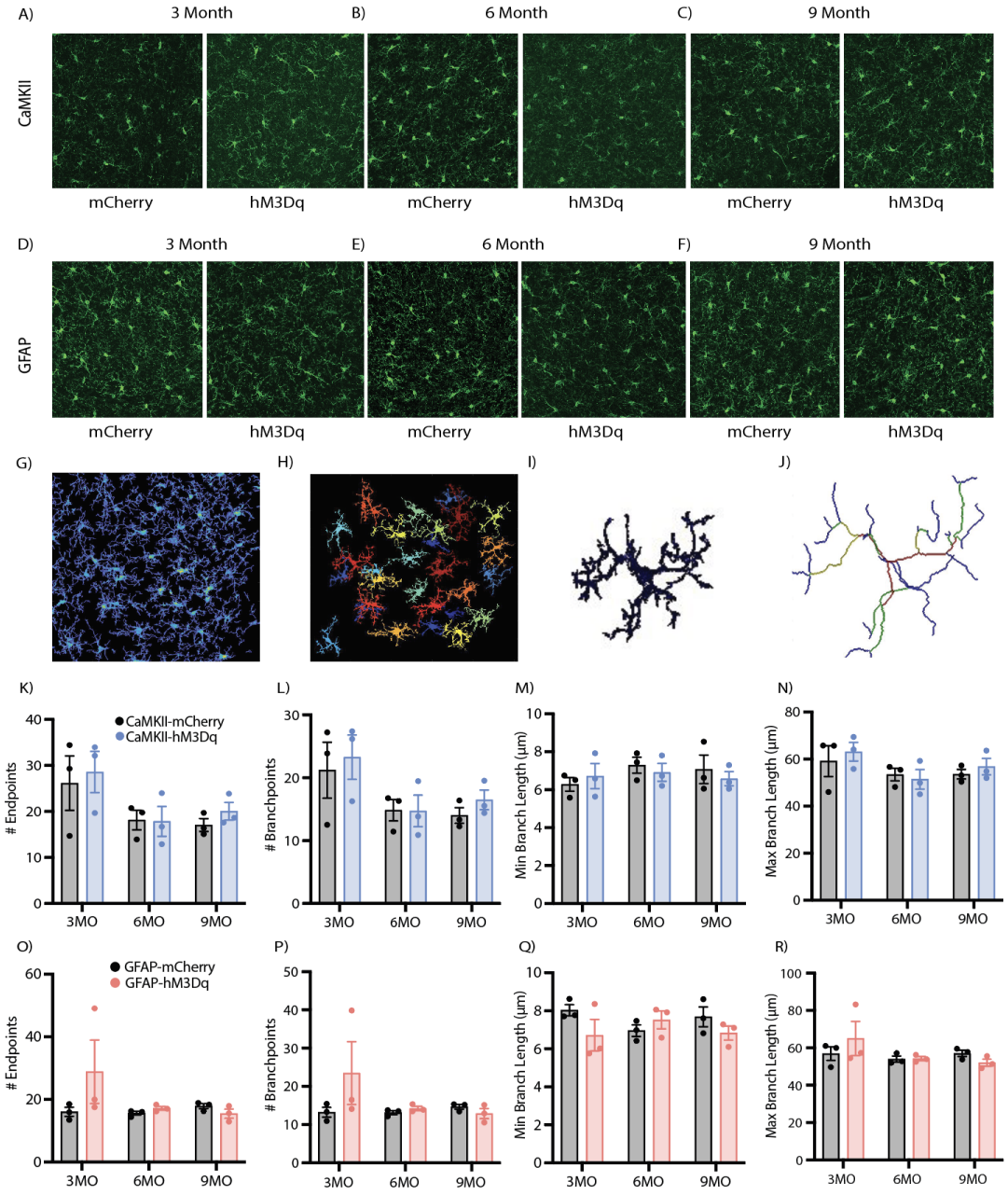

Supplemental Figure 5: Microglial morphology in vCA1 showed no significant differences with Gq activation of CaMKII+ or GFAP+ cells in vHPC. (A-C) Representative hippocampal ventral CA1 Iba-1 (green) expression for CaMKII-mCherry and hM3Dq groups for the 3 month (A), 6 month (B) and 9 month (C) timepoints to quantify cell number and morphological changes between groups and across time points. (D-F) Representative hippocampal ventral CA1 Iba-1 (green) expression for GFAP-mCherry and hM3Dq groups for the 3 month (D), 6 month (E) and 9 month (F) timepoints. (G-J) Representative image processing in 3DMorph; 2-dimensional (2D) threshold map generated from threshold and noise filtering parameters of a 3-dimensional (3D) z-stack image (G), isolated full cells generated by maximum and minimum cell size

parameters (H), individual full cell (I), and skeletonized full cell used to generate outputs (e.g. territorial volume, cell size, ramification index) (J). (K-N) Quantification of remaining Iba-1+ morphological metrics; number of endpoints (K), number of branch points (L), minimum branch length (M) and maximum branch length (N) for the 3, 6 and 9 month CaMKII-mCherry and hM3Dq groups. (O-R) Quantification of remaining Iba-1+ morphological metrics; number of endpoints (O), number of branch points (P), minimum branch length (Q) and maximum branch length (R) for the 3, 6 and 9 month GFAP-mCherry and hM3Dq groups. Microglial morphology metrics were assessed with a two-way analysis of variance (ANOVA) with time point and group as factors. Tukey's *post hoc* tests were performed where applicable. Error bars indicate SEM. $p \leq 0.05$, $^{**}p \leq 0.01$, $^{***}p \leq 0.001$, $^{****}p \leq 0.0001$, ns = not significant. All groups: n= 3 mice x 18 tiles (ROI: vCA1) each were quantified for statistical analysis of astrocytic and microglial morphology per group.

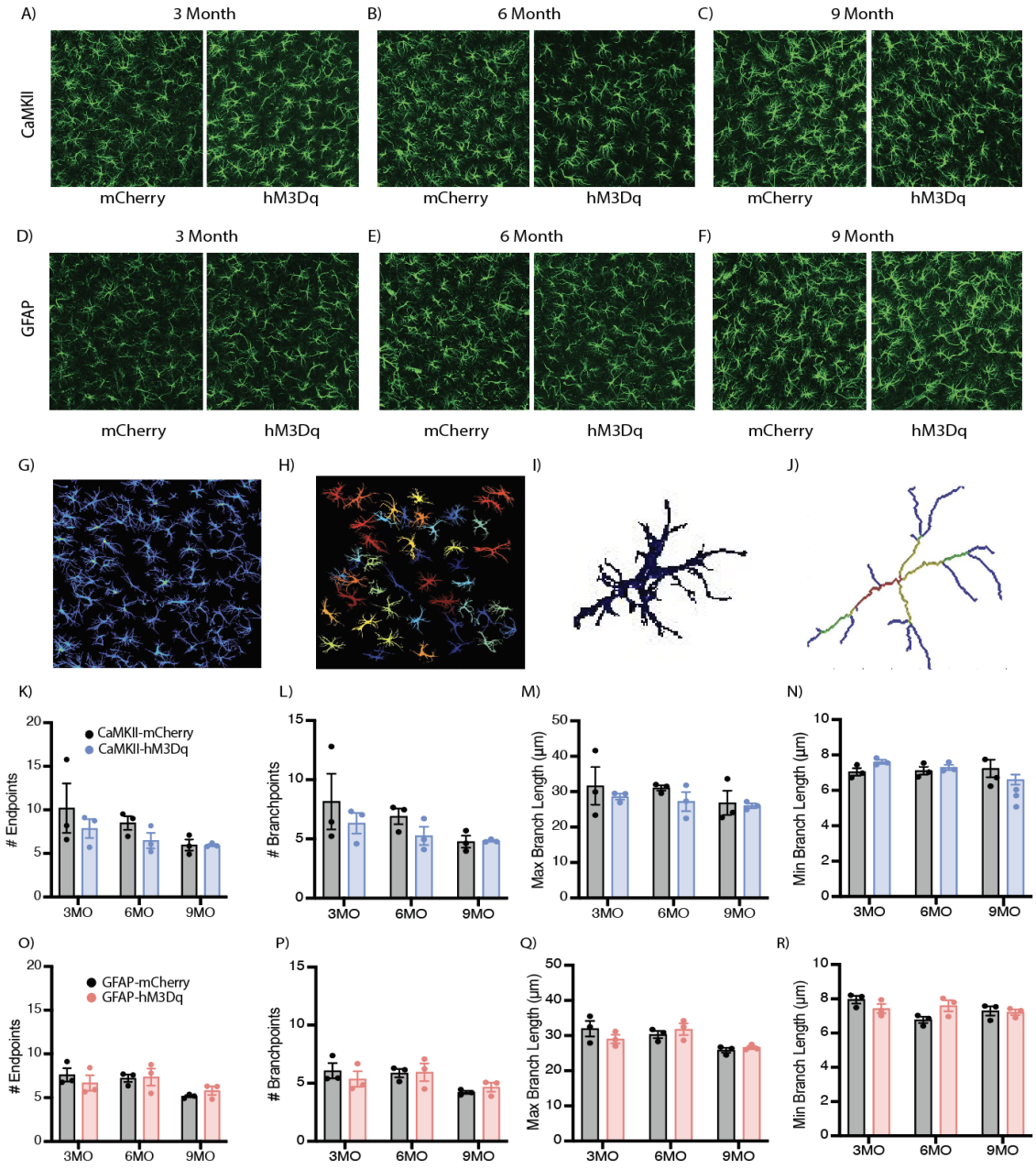

Supplemental Figure 6: Astrocytic morphology in vCA1 showed no significant differences with Gq activation of CaMKII+ or GFAP+ cells in vHPC. (A-C) Representative hippocampal ventral CA1 GFAP (green) expression for CaMKII-mCherry and hM3Dq groups for the 3 month (A), 6 month (B) and 9 month (C) timepoints to quantify cell number and morphological changes between groups and across time points. (D-F) Representative hippocampal ventral CA1 GFAP (green) expression for GFAP-mCherry and hM3Dq groups for the 3 month (D), 6 month (E) and 9 month (F) timepoints. (G-J) Representative image processing in 3DMorph; 2-dimensional (2D) threshold map generated from threshold and noise filtering parameters of a 3-dimensional (3D) z-stack image (G), isolated full cells generated by maximum and minimum cell size

parameters (H), individual full cell (I), and skeletonized full cell used to generate outputs (e.g. territorial volume, cell size, ramification index) (J). (K-N) Quantification of remaining GFAP+ cell morphological metrics; number of endpoints (K), number of branch points (L), minimum branch length (M) and maximum branch length (N) for the 3, 6 and 9 month CaMKII-mCherry and hM3Dq groups. (O-R) Quantification of remaining GFAP+ cell morphological metrics; number of endpoints (O), number of branch points (P), minimum branch length (Q) and maximum branch length (R) for the 3, 6 and 9 month GFAP-mCherry and hM3Dq groups. Astrocytic morphology metrics were assessed with a two-way analysis of variance (ANOVA) with time point and group as factors. Tukey's *post hoc* tests were performed where applicable. Error bars indicate SEM. $p \leq 0.05$, $^{**}p \leq 0.01$, $^{***}p \leq 0.001$, $^{****}p \leq 0.0001$, ns = not significant. All groups: n= 3 mice x 18 tiles (ROI: vCA1) each were quantified for statistical analysis of astrocytic and microglial morphology per group.

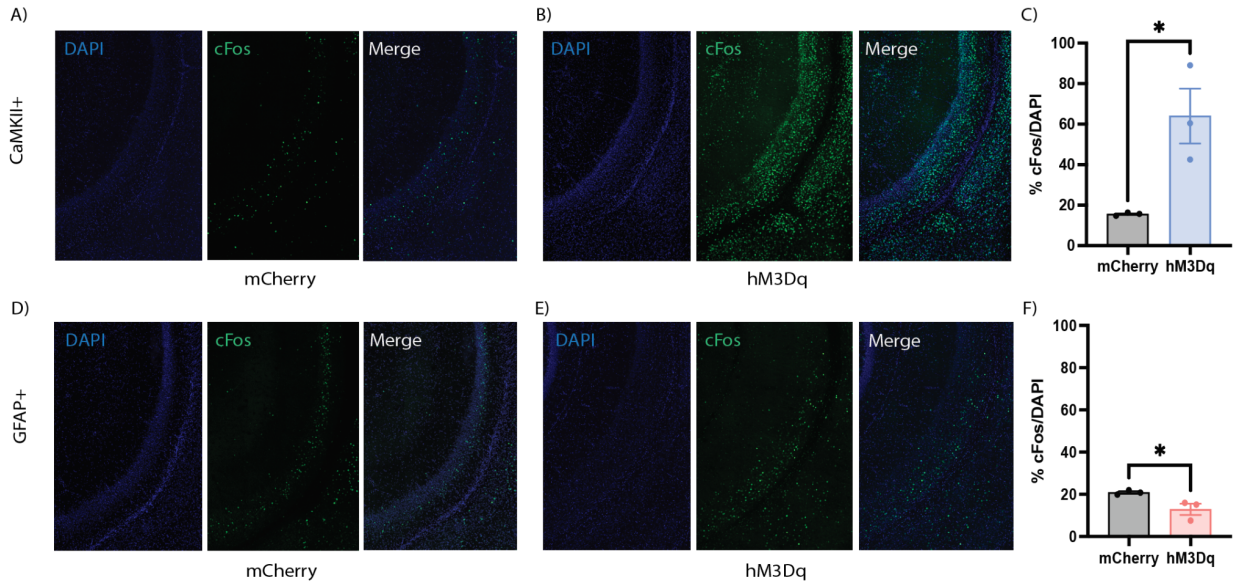

Supplemental Figure 7. Gq activation with intraperitoneal (i.p.) administration of deschloroclozapine (DCZ) of GFAP+ cells decreases vHPC cFos levels in the pyramidal cell layer, while activation of CaMKII+ cells increases cFos levels. (A-B) Representative hippocampal ventral CA1 expression of DAPI and cFos expression in the CaMKII-mCherry (left) and CaMKII-hM3Dq (right) groups. (C) Quantification of % cFos/DAPI in the pyramidal cell layer for CaMKII groups. (D-E) Representative hippocampal ventral CA1 expression of DAPI and cFos expression in the GFAP-mCherry (left) and GFAP-hM3Dq (right) groups. (F) Quantification of % cFos/DAPI in the vCA1 pyramidal layer for GFAP groups. All groups: n= 3 mice x 4 slices (ROI: vCA1 pyramidal cell layer) each were quantified for statistical analysis of cFos/DAPI counts per group. Error bars indicate SEM. For independent t-tests, $p \leq 0.05$, $^{**}p \leq 0.01$, $^{***}p \leq 0.001$, $^{****}p \leq 0.0001$, ns = not significant.

5) References.

Adamsky, A., Kol, A., Kreisel, T., Doron, A., Ozeri-Engelhard, N., Melcer, T., Refaeli, R., Horn, H., Regev, L., Groysman, M., London, M., Goshen, I., 2018. Astrocytic Activation Generates De Novo Neuronal Potentiation and Memory Enhancement. Cell 174, 59-71.e14. https://doi.org/10.1016/j.cell.2018.05.002

Anastacio, H.T.D., Matosin, N., Ooi, L., 2022. Neuronal hyperexcitability in Alzheimer's disease: what are the drivers behind this aberrant phenotype? Transl Psychiatry 12, 257. https://doi.org/10.1038/s41398-022-02024-7

Aqrabawi, A.J., Kim, J.C., 2018. Behavioral Evaluation of Odor Memory in Mice. Bio Protoc 8. https://doi.org/10.21769/BIOPROTOC.3023

Araque, A., Carmignoto, G., Haydon, P.G., 2001. Dynamic signaling between astrocytes and neurons. Annu Rev Physiol 63, 795–813. https://doi.org/10.1146/ANNUREV.PHYSIOL.63.1.795

Araque, A., Parpura, V., Sanzgiri, R.P., Haydon, P.G., 1999. Tripartite synapses: Glia, the unacknowledged partner. Trends Neurosci 22, 208–215. https://doi.org/10.1016/S0166-2236(98)01349-6

Badura-Brack, A., McDermott, T.J., Heinrichs-Graham, E., Ryan, T.J., Khanna, M.M., Pine, D.S., Bar-Haim, Y., Wilson, T.W., 2018. Veterans with PTSD Demonstrate Amygdala Hyperactivity while Viewing Threatening Faces: A MEG Study. Biol Psychol 132, 228. https://doi.org/10.1016/J.BIOPSYCHO.2018.01.005

Bennett, D.A., Schneider, J.A., Tang, Y., Arnold, S.E., Wilson, R.S., 2006. The effect of social networks on the relation between Alzheimer's disease pathology and level of cognitive function in old people: a longitudinal cohort study. Lancet Neurol 5, 406–412. https://doi.org/10.1016/S1474-4422(06)70417-3

Berg, S., Kutra, D., Kroeger, T., Straehle, C.N., Kausler, B.X., Haubold, C., Schiegg, M., Ales, J., Beier, T., Rudy, M., Eren, K., Cervantes, J.I., Xu, B., Beuttenmueller, F., Wolny, A., Zhang, C., Koethe, U., Hamprecht, F.A., Kreshuk, A., 2019. ilastik: interactive machine learning for (bio)image analysis. Nature Methods 2019 16:12 16, 1226–1232. https://doi.org/10.1038/s41592-019-0582-9

Berron, D., Cardenas-Blanco, A., Bittner, D., Metzger, C.D., Spottke, A., Heneka, M.T., Fliessbach, K., Schneider, A., Teipel, S.J., Wagner, M., Speck, O., Jessen, F., Duzel, E., 2019. Higher CSF Tau Levels Are Related to Hippocampal Hyperactivity and Object Mnemonic Discrimination in Older Adults. Journal of Neuroscience 39, 8788–8797. https://doi.org/10.1523/JNEUROSCI.1279-19.2019

Bezzi, P., Volterra, A., 2001. A neuron-glia signalling network in the active brain. Curr Opin Neurobiol 11, 387–394. https://doi.org/10.1016/S0959-4388(00)00223-3

Bi, D., Wen, L., Wu, Z., Shen, Y., 2020. GABAergic dysfunction in excitatory and inhibitory (E/I) imbalance drives the pathogenesis of Alzheimer's disease. Alzheimer's & Dementia 16, 1312–1329. https://doi.org/10.1002/ALZ.12088

Bonaventura, J., Eldridge, M.A.G., Hu, F., Gomez, J.L., Sanchez-Soto, M., Abramyan, A.M., Lam, S., Boehm, M.A., Ruiz, C., Farrell, M.R., Moreno, A., Faress, I.M.G., Andersen, N., Lin, J.Y., Moaddel, R., Morris, P.J., Shi, L., Sibley, D.R., Mahler, S. v, Nabavi, S., Pomper, M.G., Bonci, A., Horti, A.G., Richmond, B.J., Michaelides, M., 2019. High-potency ligands for DREADD imaging and activation in rodents and monkeys. Nat Commun 10. https://doi.org/10.1038/s41467-019-12236-z

Braak, H., Braak, E., 1991. Neuropathological stageing of Alzheimer-related changes. Acta Neuropathol 82, 239–259. https://doi.org/10.1007/BF00308809

Broadbent, N.J., Squire, L.R., Clark, R.E., 2004. Spatial memory, recognition memory, and the hippocampus. Proc Natl Acad Sci U S A 101, 14515–14520. https://doi.org/10.1073/PNAS.0406344101/SUPPL_FILE/06344FIG8.PDF

Brys, M., Fox, M.D., Agarwal, S., Biagioni, M., Dacpano, G., Kumar, P., Pirraglia, E., Chen, R., Wu, A., Fernandez, H., Shukla, A.W., Lou, J.S., Gray, Z., Simon, D.K., Rocco, A. di, Pascual-Leone, A., 2016. Multifocal repetitive TMS for motor and mood symptoms of Parkinson disease: A randomized trial. Neurology 87, 1907. https://doi.org/10.1212/WNL.0000000000003279

Burgess, N., Maguire, E.A., O'Keefe, J., 2002. The human hippocampus and spatial and episodic memory. Neuron 35, 625–641. https://doi.org/10.1016/S0896-6273(02)00830-9

Busche, M.A., Chen, X., Henning, H.A., Reichwald, J., Staufenbiel, M., Sakmann, B., Konnerth, A., 2012. Critical role of soluble amyloid-β for early hippocampal hyperactivity in a mouse model of Alzheimer's disease. Proc Natl Acad Sci U S A 109, 8740–8745. https://doi.org/10.1073/PNAS.1206171109

Busche, M.A., Eichhoff, G., Adelsberger, H., Abramowski, D., Wiederhold, K.H., Haass, C., Staufenbiel, M., Konnerth, A., Garaschuk, O., 2008. Clusters of hyperactive neurons near amyloid plaques in a mouse model of Alzheimer's disease. Science (1979) 321, 1686–1689. https://doi.org/10.1126/SCIENCE.1162844

Byers, A.L., Yaffe, K., 2011. Depression and Risk of Developing Dementia. Nat Rev Neurol 7, 323. https://doi.org/10.1038/NRNEUROL.2011.60

Campanelli, F., Natale, G., Marino, G., Ghiglieri, V., Calabresi, P., 2022. Striatal glutamatergic hyperactivity in Parkinson's disease. Neurobiol Dis 168, 105697. https://doi.org/10.1016/J.NBD.2022.105697

Castellani, R.J., Perry, G., Tabaton, M., 2019. Tau Biology, Tauopathy, Traumatic Brain Injury, and Diagnostic Challenges. Journal of Alzheimer's Disease 67, 447. https://doi.org/10.3233/JAD-180721

Chen, N., Sugihara, H., Kim, J., Fu, Z., Barak, B., Sur, M., Feng, G., Han, W., 2016. Direct modulation of GFAP-expressing glia in the arcuate nucleus bi-directionally regulates feeding. Elife 5. https://doi.org/10.7554/ELIFE.18716

Ciocchi, S., Passecker, J., Malagon-Vina, H., Mikus, N., Klausberger, T., 2015. Selective information routing by ventral hippocampal CA1 projection neurons. Science (1979) 348, 560–563. https://doi.org/10.1126/SCIENCE.AAA3245/SUPPL_FILE/AAA3245-CIOCCHI-SM.PDF

Clancy, K., Ding, M., Bernat, E., Schmidt, N.B., Li, W., 2017. Restless 'rest': intrinsic sensory hyperactivity and disinhibition in post-traumatic stress disorder. Brain 140, 2041–2050. https://doi.org/10.1093/BRAIN/AWX116

Clark, R.E., Broadbent, N.J., Squire, L.R., 2005. Impaired Remote Spatial Memory After Hippocampal Lesions Despite Extensive Training Beginning Early in Life. Hippocampus 15, 340. https://doi.org/10.1002/HIPO.20076

Cole, J.C., Bernacki, C.G., Helmer, A., Pinninti, N., O'Reardon, J.P., 2015. Efficacy of Transcranial Magnetic Stimulation (TMS) in the Treatment of Schizophrenia: A Review of the Literature to Date. Innov Clin Neurosci 12, 12.

Covelo, A., Araque, A., 2018. Neuronal activity determines distinct gliotransmitter release from a single astrocyte. Elife 7. https://doi.org/10.7554/ELIFE.32237

Dehouck, M. -P, Méresse, S., Delorme, P., Fruchart, J. -C, Cecchelli, R., 1990. An Easier, Reproducible, and Mass-Production Method to Study the Blood–Brain Barrier In Vitro. J Neurochem 54, 1798–1801. https://doi.org/10.1111/J.1471-4159.1990.TB01236.X

Deisseroth, K., 2014. Circuit dynamics of adaptive and maladaptive behaviour. Nature 2014 505:7483 505, 309–317. https://doi.org/10.1038/nature12982

di Castro, M.A., Chuquet, J., Liaudet, N., Bhaukaurally, K., Santello, M., Bouvier, D., Tiret, P., Volterra, A., 2011. Local Ca2+ detection and modulation of synaptic release by astrocytes. Nat Neurosci 14, 1276–1284. https://doi.org/10.1038/NN.2929

Durkee, C.A., Covelo, A., Lines, J., Kofuji, P., Aguilar, J., Araque, A., 2019. Gi/o protein-coupled receptors inhibit neurons but activate astrocytes and stimulate gliotransmission. Glia 67, 1076–1093. https://doi.org/10.1002/GLIA.23589

Eichenbaum, H., Fortin, N., 2016. Episodic Memory and the Hippocampus: It's About Time. https://doi.org/10.1111/1467-8721.01225 12, 53–57. https://doi.org/10.1111/1467-8721.01225

Eichenbaum, H., Otto, T., Cohen, N.J., 1992. The hippocampus-what does it do? Behav Neural Biol 57, 2–36. https://doi.org/10.1016/0163-1047(92)90724-I

Ellwardt, E., Pramanik, G., Luchtman, D., Novkovic, T., Jubal, E.R., Vogt, J., Arnoux, I., Vogelaar, C.F., Mandal, S., Schmalz, M., Barger, Z., de Azua, I.R., Kuhlmann, T., Lutz, B., Mittmann, T., Bittner, S., Zipp, F., Stroh, A., 2018. Maladaptive cortical hyperactivity upon recovery from experimental autoimmune encephalomyelitis. Nature Neuroscience 2018 21:10 21, 1392–1403. https://doi.org/10.1038/s41593-018-0193-2

Fang, Q., Li, Z., Huang, G.-D., Zhang, H.-H., Chen, Y.-Y., Zhang, L.-B., Ding, Z.-B., Shi, J., Lu, L., Yang, J.-L., 2018. Traumatic Stress Produces Distinct Activations of GABAergic and Glutamatergic Neurons in Amygdala. Front Neurosci 12. https://doi.org/10.3389/fnins.2018.00387

Fanselow, M.S., Dong, H.W., 2010. Are the dorsal and ventral hippocampus functionally distinct structures? Neuron 65, 7–19. https://doi.org/10.1016/J.NEURON.2009.11.031

Fellin, T., Pascual, O., Gobbo, S., Pozzan, T., Haydon, P.G., Carmignoto, G., 2004. Neuronal synchrony mediated by astrocytic glutamate through activation of extrasynaptic NMDA receptors. Neuron 43, 729–743. https://doi.org/10.1016/j.neuron.2004.08.011

Figley, C.R., Stroman, P.W., 2011. The role(s) of astrocytes and astrocyte activity in neurometabolism, neurovascular coupling, and the production of functional neuroimaging signals. European Journal of Neuroscience 33, 577–588. https://doi.org/10.1111/J.1460-9568.2010.07584.X

Flatt, J.D., Gilsanz, P., Quesenberry, C.P., Albers, K.B., Whitmer, R.A., 2018. Post-traumatic stress disorder and risk of dementia among members of a healthcare delivery system. Alzheimers Dement 14, 28. https://doi.org/10.1016/J.JALZ.2017.04.014

Gauthier, S., Boxer, A., Knopman, D., Sims, J., Doody, R., Aisen, P., Iwatsubo, T., Bateman, R., Vellas, B., 2022. Therapeutic Targets for Alzheimer's Disease: Amyloid Vs. Non-Amyloid. Where Does Consensus Lie Today? An CTAD Task Force Report. Journal of Prevention of Alzheimer's Disease 9, 231–235. https://doi.org/10.14283/JPAD.2022.29/TABLES/1

Gergues, M.M., Han, K.J., Choi, H.S., Brown, B., Clausing, K.J., Turner, V.S., Vainchtein, I.D., Molofsky, A. v., Kheirbek, M.A., 2020. Circuit and molecular architecture of a ventral hippocampal network. Nature Neuroscience 2020 23:11 23, 1444–1452. https://doi.org/10.1038/s41593-020-0705-8

Haydon, P.G., 2001. Glia: listening and talking to the synapse. Nature Reviews Neuroscience 2001 2:3 2, 185–193. https://doi.org/10.1038/35058528

Heckers, S., Konradi, C., 2015. GABAergic mechanisms of hippocampal hyperactivity in schizophrenia. Schizophr Res 167, 4. https://doi.org/10.1016/J.SCHRES.2014.09.041

Helm, K., Viol, K., Weiger, T.M., Tass, P.A., Grefkes, C., del Monte, D., Schiepek, G., 2018. Neuronal connectivity in major depressive disorder: a systematic review. Neuropsychiatr Dis Treat Volume 14, 2715–2737. https://doi.org/10.2147/NDT.S170989

Jang, J.S., Choi, C. il, Yi, J., Butters, K., Kim, I., Bhagwate, A., Jen, J., Chang, S. youne, 2019. High frequency electrical stimulation promotes expression of extracellular matrix proteins from human astrocytes. Mol Biol Rep 46, 4369–4375. https://doi.org/10.1007/S11033-019-04890-9

Jennings, J.H., Sparta, D.R., Stamatakis, A.M., Ung, R.L., Pleil, K.E., Kash, T.L., Stuber, G.D., 2013. Distinct extended amygdala circuits for divergent motivational states. Nature 2013 496:7444 496, 224–228. https://doi.org/10.1038/nature12041

Jimenez, Jessica C, Berry, J.E., Lim, S.C., Ong, S.K., Kheirbek, M.A., Hen, R., 2020. Contextual fear memory retrieval by correlated ensembles of ventral CA1 neurons. Nat Commun 11. https://doi.org/10.1038/s41467-020-17270-w

Jimenez, Jessica C., Berry, J.E., Lim, S.C., Ong, S.K., Kheirbek, M.A., Hen, R., 2020. Contextual fear memory retrieval by correlated ensembles of ventral CA1 neurons. Nat Commun 11. https://doi.org/10.1038/S41467-020-17270-W

Johnson, M.D., Lim, H.H., Netoff, T.I., Connolly, A.T., Johnson, N., Roy, A., Holt, A., Lim, K.O., Carey, J.R., Vitek, J.L., He, B., 2013. Neuromodulation for Brain Disorders: Challenges and Opportunities. IEEE Trans Biomed Eng 60, 610–624. https://doi.org/10.1109/TBME.2013.2244890

Karaca, K.G., Kupke, J., Brito, D.V.C., Zeuch, B., Thome, C., Weichenhan, D., Lutsik, P., Plass, C., Oliveira, A.M.M., 2020. Neuronal ensemble-specific DNA methylation strengthens engram stability. Nat Commun 11. https://doi.org/10.1038/s41467-020-14498-4

Klink, K., Jaun, U., Federspiel, A., Wunderlin, M., Teunissen, C.E., Kiefer, C., Wiest, R., Scharnowski, F., Sladky, R., Haugg, A., Hellrung, L., Peter, J., 2021. Targeting hippocampal hyperactivity with real-time

fMRI neurofeedback: protocol of a single-blind randomized controlled trial in mild cognitive impairment. BMC Psychiatry 21, 1–9. https://doi.org/10.1186/S12888-021-03091-8/FIGURES/4

Kofuji, P., Newman, E.A., 2004. Potassium buffering in the central nervous system. Neuroscience 129, 1043–1054. https://doi.org/10.1016/J.NEUROSCIENCE.2004.06.008

Koizumi, S., Fujishita, K., Inoue, K., n.d. Regulation of cell-to-cell communication mediated by astrocytic ATP in the CNS. https://doi.org/10.1007/s11302-005-6321-y

Kol, A., Adamsky, A., Groysman, M., Kreisel, T., London, M., Goshen, I., 2020. Astrocytes Contribute to Remote Memory Formation by Modulating Hippocampal-Cortical Communication During Learning. Nat Neurosci 23, 1229. https://doi.org/10.1038/S41593-020-0679-6

Kuchibhotla, K. v., Lattarulo, C.R., Hyman, B.T., Bacskai, B.J., 2009. Synchronous Hyperactivity and Intercellular Calcium Waves in Astrocytes in Alzheimer Mice. Science 323, 1211. https://doi.org/10.1126/SCIENCE.1169096

Lauterborn, J.C., Scaduto, P., Cox, C.D., Schulmann, A., Lynch, G., Gall, C.M., Keene, C.D., Limon, A., 2021. Increased excitatory to inhibitory synaptic ratio in parietal cortex samples from individuals with Alzheimer's disease. Nature Communications 2021 12:1 12, 1–15. https://doi.org/10.1038/s41467-021-22742-8

Lei, Z., Xie, L., Li, C.H., Lam, Y.Y., Ramkrishnan, A.S., Fu, Z., Zeng, X., Liu, S., Iqbal, Z., Li, Y., 2022. Chemogenetic Activation of Astrocytes in the Basolateral Amygdala Contributes to Fear Memory Formation by Modulating the Amygdala & Prefrontal Cortex Communication. International Journal of Molecular Sciences 2022, Vol. 23, Page 6092 23, 6092. https://doi.org/10.3390/IJMS23116092

Lerdkrai, C., Asavapanumas, N., Brawek, B., Kovalchuk, Y., Mojtahedi, N., del Moral, M.O., Garaschuk, O., 2018. Intracellular Ca2+ stores control in vivo neuronal hyperactivity in a mouse model of Alzheimer's disease. Proc Natl Acad Sci U S A 115, E1279–E1288. https://doi.org/10.1073/PNAS.1714409115/SUPPL_FILE/PNAS.201714409SI.PDF

Liddelow, S. A., Marsh, S. E., & Stevens, B. (2020). Microglia and Astrocytes in Disease: Dynamic Duo or Partners in Crime? Trends in Immunology, 41(9), 820–835. https://doi.org/10.1016/j.it.2020.07.006

Li, Y., Li, L., Wu, J., Zhu, Z., Feng, X., Qin, L., Zhu, Y., Sun, L., Liu, Y., Qiu, Z., Duan, S., Yu, Y.Q., 2020. Activation of astrocytes in the hippocampus decreases fear memory through adenosine A1 receptors. Elife 9, 1–25. https://doi.org/10.7554/ELIFE.57155

Martin-Fernandez, M., Jamison, S., Robin, L.M., Zhao, Z., Martin, E.D., Aguilar, J., Benneyworth, M.A., Marsicano, G., Araque, A., 2017. Synapse-specific astrocyte gating of amygdala-related behavior. Nat Neurosci 20, 1540. https://doi.org/10.1038/NN.4649

Martín-Sánchez, A., Piñero, J., Nonell, L., Arnal, M., Ribe, E.M., Nevado-Holgado, A., Lovestone, S., Sanz, F., Furlong, L.I., Valverde, O., 2021. Comorbidity between Alzheimer's disease and major depression: a behavioural and transcriptomic characterization study in mice. Alzheimers Res Ther 13, 73. https://doi.org/10.1186/s13195-021-00810-x

Maruszak, A., Thuret, S., 2014. Why looking at the whole hippocampus is not enough-a critical role for anteroposterior axis, subfield and activation analyses to enhance predictive value of hippocampal changes

for Alzheimer's disease diagnosis. Front Cell Neurosci 8, 95. https://doi.org/10.3389/FNCEL.2014.00095/BIBTEX

Matyash, V., Kettenmann, H., 2010. Heterogeneity in astrocyte morphology and physiology. Brain Res Rev 63, 2–10. https://doi.org/10.1016/J.BRAINRESREV.2009.12.001

Mederos, S., Sánchez-Puelles, C., Esparza, J., Valero, M., Ponomarenko, A., Perea, G., 2021. GABAergic signaling to astrocytes in the prefrontal cortex sustains goal-directed behaviors. Nat Neurosci 24, 82–92. https://doi.org/10.1038/S41593-020-00752-X

Mohamed, N.V., Desjardins, A., Leclerc, N., 2017. Tau secretion is correlated to an increase of Golgi dynamics. PLoS One 12, e0178288. https://doi.org/10.1371/JOURNAL.PONE.0178288

Moser, M.-B., Moser, E.I., 1998. Functional differentiation in the hippocampus. Hippocampus 8, 608–619. https://doi.org/10.1002/(SICI)1098-1063(1998)8:6<608::AID-HIPO3>3.0.CO;2-7

Nagai, J., Rajbhandari, A.K., Gangwani, M.R., Hachisuka, A., Coppola, G., Masmanidis, S.C., Fanselow, M.S., Khakh, B.S., 2019. Hyperactivity with Disrupted Attention by Activation of an Astrocyte Synaptogenic Cue. Cell 177, 1280-1292.e20. https://doi.org/10.1016/J.CELL.2019.03.019

Nagai, Y., Miyakawa, N., Takuwa, H., Hori, Y., Oyama, K., Ji, B., Takahashi, M., Huang, X.P., Slocum, S.T., DiBerto, J.F., Xiong, Y., Urushihata, T., Hirabayashi, T., Fujimoto, A., Mimura, K., English, J.G., Liu, J., Inoue, K. ichi, Kumata, K., Seki, C., Ono, M., Shimojo, M., Zhang, M.R., Tomita, Y., Nakahara, J., Suhara, T., Takada, M., Higuchi, M., Jin, J., Roth, B.L., Minamimoto, T., 2020. Deschloroclozapine, a potent and selective chemogenetic actuator enables rapid neuronal and behavioral modulations in mice and monkeys. Nature Neuroscience 2020 23:9 23, 1157–1167. https://doi.org/10.1038/s41593-020-0661-3

Nasios, G., Bakirtzis, C., Messinis, L., 2020. Cognitive Impairment and Brain Reorganization in MS: Underlying Mechanisms and the Role of Neurorehabilitation. Front Neurol 11, 147. https://doi.org/10.3389/FNEUR.2020.00147/XML/NLM

Neddens, J., Daurer, M., Loeffler, T., Alzola Aldamizetxebarria, S., Flunkert, S., Hutter-Paier, B., 2020. Constant Levels of Tau Phosphorylation in the Brain of htau Mice. Front Mol Neurosci 13. https://doi.org/10.3389/FNMOL.2020.00136/FULL

Neddens, J., Temmel, M., Flunkert, S., Kerschbaumer, B., Hoeller, C., Loeffler, T., Niederkofler, V., Daum, G., Attems, J., Hutter-Paier, B., 2018. Phosphorylation of different tau sites during progression of Alzheimer's disease. Acta Neuropathol Commun 6, 52. https://doi.org/10.1186/S40478-018-0557-6/FIGURES/8

Oberheim, N.A., Goldman, S.A., Nedergaard, M., 2012. Heterogeneity of astrocytic form and function. Methods in Molecular Biology 814, 23–45. https://doi.org/10.1007/978-1-61779-452-0_3/COVER

Oizumi, H., Kuriyama, N., Imamura, S., Tabuchi, M., Omiya, Y., Mizoguchi, K., Kobayashi, H., 2019. Influence of aging on the behavioral phenotypes of C57BL/6J mice after social defeat. PLoS One 14. https://doi.org/10.1371/JOURNAL.PONE.0222076

Okuyama, T., Kitamura, T., Roy, D.S., Itohara, S., Tonegawa, S., 2016. Ventral CA1 neurons store social memory. Science (1979) 353, 1536–1541. https://doi.org/10.1126/SCIENCE.AAF7003/SUPPL_FILE/OKUYAMA.SM.PDF

Ownby, R.L., Crocco, E., Acevedo, A., John, V., Loewenstein, D., 2006. Depression and risk for Alzheimer disease: systematic review, meta-analysis, and metaregression analysis. Arch Gen Psychiatry 63, 530–538. https://doi.org/10.1001/ARCHPSYC.63.5.530

Padilla-Coreano, N., Bolkan, S.S., Pierce, G.M., Blackman, D.R., Hardin, W.D., Garcia-Garcia, A.L., Spellman, T.J., Gordon, J.A., 2016. Direct Ventral Hippocampal-Prefrontal Input Is Required for Anxiety-Related Neural Activity and Behavior. Neuron 89, 857–866. https://doi.org/10.1016/j.neuron.2016.01.011

Palop, J.J., Chin, J., Roberson, E.D., Wang, J., Thwin, M.T., Bien-Ly, N., Yoo, J., Ho, K.O., Yu, G.Q., Kreitzer, A., Finkbeiner, S., Noebels, J.L., Mucke, L., 2007. Aberrant excitatory neuronal activity and compensatory remodeling of inhibitory hippocampal circuits in mouse models of Alzheimer's disease. Neuron 55, 697–711. https://doi.org/10.1016/J.NEURON.2007.07.025

Palop, J.J., Mucke, L., 2016. Network abnormalities and interneuron dysfunction in Alzheimer disease. Nature Reviews Neuroscience 2016 17:12 17, 777–792. https://doi.org/10.1038/nrn.2016.141

Parpura, V., Basarsky, T.A., Liu, F., Jeftinija, K., Jeftinija, S., Haydon, P.G., 1994. Glutamate-mediated astrocyte-neuron signaling. Nature 369, 744–747. https://doi.org/10.1038/369744A0

Paulson, O.B., Newman, E.A., 1987. Does the release of potassium from the astrocyte endfeet regulate cerebral blood flow? Science 237, 896–898. https://doi.org/10.1126/SCIENCE.3616619

Perea, G., Araque, A., 2005. Glial calcium signaling and neuron–glia communication. Cell Calcium 38, 375–382. https://doi.org/10.1016/J.CECA.2005.06.015

Perea, G., Navarrete, M., Araque, A., 2009. Tripartite synapses: astrocytes process and control synaptic information. Trends Neurosci 32, 421–431. https://doi.org/10.1016/J.TINS.2009.05.001

Phillips, M.L., Robinson, H.A., Pozzo-Miller, L., 2019. Ventral hippocampal projections to the medial prefrontal cortex regulate social memory. Elife 8. https://doi.org/10.7554/ELIFE.44182

Pi, G., Gao, D., Wu, D., Wang, Y., Lei, H., Zeng, W., Gao, Y., Yu, H., Xiong, R., Jiang, T., Li, S., Wang, X., Guo, J., Zhang, S., Yin, T., He, T., Ke, D., Li, R., Li, H., Liu, G., Yang, X., Luo, M. –H, Zhang, X., Yang, Y., Wang, J. –Z, 2020. Posterior basolateral amygdala to ventral hippocampal CA1 drives approach behaviour to exert an anxiolytic effect. Nat Commun 11. https://doi.org/10.1038/s41467-019-13919-3

Porter, J.T., McCarthy, K.D., 1997. ASTROCYTIC NEUROTRANSMITTER RECEPTORS IN SITU AND IN VIVO. Prog Neurobiol 51, 439–455. https://doi.org/10.1016/S0301-0082(96)00068-8

Rouach, N., Koulakoff, A., Abudara, V., Willecke, K., Giaume, C., 2008. Astroglial metabolic networks sustain hippocampal synaptic transmission. Science (1979) 322, 1551–1555. https://doi.org/10.1126/SCIENCE.1164022/SUPPL_FILE/ROUACH.SOM.PDF

Schmidt Buosi, A., Matias, I., Paula, A., Araujo, B., Batista, C., Carvalho, F., Gomes, A., 2035. Heterogeneity in Synaptogenic Profile of Astrocytes from Different Brain Regions. https://doi.org/10.1007/s12035-016-0343-z

Seibenhener, M.L., Wooten, M.C., 2015. Use of the Open Field Maze to measure locomotor and anxiety-like behavior in mice. J Vis Exp. https://doi.org/10.3791/52434

Shelkar, G.P., Liu, J., Dravid, S.M., 2021. Astrocytic NMDA Receptors in the Basolateral Amygdala Contribute to Facilitation of Fear Extinction. International Journal of Neuropsychopharmacology 24, 907–919. https://doi.org/10.1093/IJNP/PYAB055

Shoji, H., Takao, K., Hattori, S., Miyakawa, T., 2016. Age-related changes in behavior in C57BL/6J mice from young adulthood to middle age. Molecular Brain 2016 9:1 9, 1–18. https://doi.org/10.1186/S13041-016-0191-9

Simard, M., Nedergaard, M., 2004. The neurobiology of glia in the context of water and ion homeostasis. Neuroscience 129, 877–896. https://doi.org/10.1016/J.NEUROSCIENCE.2004.09.053

Skucas, V.A., Mathews, I.B., Yang, J., Cheng, Q., Treister, A., Duffy, A.M., Verkman, A.S., Hempstead, B.L., Wood, M.A., Binder, D.K., Scharfman, H.E., 2011. Impairment of Select Forms of Spatial Memory and Neurotrophin-Dependent Synaptic Plasticity by Deletion of Glial Aquaporin-4. Journal of Neuroscience 31, 6392–6397. https://doi.org/10.1523/JNEUROSCI.6249-10.2011

Stuber, G.D., Britt, J.P., Bonci, A., 2012. Optogenetic Modulation of Neural Circuits that Underlie Reward Seeking. Biol Psychiatry 71, 1061–1067. https://doi.org/10.1016/J.BIOPSYCH.2011.11.010

Sun, X., Bernstein, M.J., Meng, M., Rao, S., Sørensen, A.T., Yao, L., Zhang, X., Anikeeva, P.O., Lin, Y., 2020. Functionally Distinct Neuronal Ensembles within the Memory Engram. Cell 181, 410-423.e17. https://doi.org/10.1016/j.cell.2020.02.055

Tsacopoulos, M., Magistretti, P.J., 1996. Metabolic coupling between glia and neurons. Journal of Neuroscience 16, 877–885. https://doi.org/10.1523/JNEUROSCI.16-03-00877.1996

Tucker, L.B., McCabe, J.T., 2017. Behavior of Male and Female C57BL/6J Mice Is More Consistent with Repeated Trials in the Elevated Zero Maze than in the Elevated Plus Maze. Front Behav Neurosci 11. https://doi.org/10.3389/FNBEH.2017.00013

Vadodaria, K.C., Ji, Y., Skime, M., Paquola, A., Nelson, T., Hall-Flavin, D., Fredlender, C., Heard, K.J., Deng, Y., Le, A.T., Dave, S., Fung, L., Li, X., Marchetto, M.C., Weinshilboum, R., Gage, F.H., 2019. Serotonin-induced hyperactivity in SSRI-resistant major depressive disorder patient-derived neurons. Molecular Psychiatry 2019 24:6 24, 795–807. https://doi.org/10.1038/s41380-019-0363-y

van den Herrewegen, Y., Sanderson, T.M., Sahu, S., de Bundel, D., Bortolotto, Z.A., Smolders, I., 2021. Side-by-side comparison of the effects of Gq- and Gi-DREADD-mediated astrocyte modulation on intracellular calcium dynamics and synaptic plasticity in the hippocampal CA1. Mol Brain 14, 1–13. https://doi.org/10.1186/S13041-021-00856-W/TABLES/1

van Lieshout, E.C.C., Jacobs, L.D., Pelsma, M., Dijkhuizen, R.M., Visser-Meily, J.M.A., 2020. Exploring the experiences of stroke patients treated with transcranial magnetic stimulation for upper limb recovery: A qualitative study. BMC Neurol 20, 1–13. https://doi.org/10.1186/S12883-020-01936-5/TABLES/2

Vico Varela, E., Etter, G., Williams, S., 2019. Excitatory-inhibitory imbalance in Alzheimer's disease and therapeutic significance. Neurobiol Dis 127, 605–615. https://doi.org/10.1016/J.NBD.2019.04.010

Wallraff, A., Köhling, R., Heinemann, U., Theis, M., Willecke, K., Steinhäuser, C., 2006. The impact of astrocytic gap junctional coupling on potassium buffering in the hippocampus. J Neurosci 26, 5438–5447. https://doi.org/10.1523/JNEUROSCI.0037-06.2006

Weiler, M., Stieger, K.C., Long, J.M., Rapp, P.R., 2020. Transcranial Magnetic Stimulation in Alzheimer's Disease: Are We Ready? eNeuro 7. https://doi.org/10.1523/ENEURO.0235-19.2019

Wu, J.W., Hussaini, S.A., Bastille, I.M., Rodriguez, G.A., Mrejeru, A., Rilett, K., Sanders, D.W., Cook, C., Fu, H., Boonen, R.A.C.M., Herman, M., Nahmani, E., Emrani, S., Figueroa, Y.H., Diamond, M.I., Clelland, C.L., Wray, S., Duff, K.E., 2016. Neuronal activity enhances tau propagation and tau pathology in vivo. Nat Neurosci 19, 1085–1092. https://doi.org/10.1038/nn.4328

Xia, Y., Xia, Y., Prokop, S., Prokop, S., Prokop, S., Prokop, S., Gorion, K.M.M., Gorion, K.M.M., Kim, J.D., Kim, J.D., Sorrentino, Z.A., Sorrentino, Z.A., Bell, B.M., Bell, B.M., Manaois, A.N., Manaois, A.N., Chakrabarty, P., Chakrabarty, P., Chakrabarty, P., Davies, P., Giasson, B.I., Giasson, B.I., Giasson, B.I., 2020. Tau Ser208 phosphorylation promotes aggregation and reveals neuropathologic diversity in Alzheimer's disease and other tauopathies. Acta Neuropathol Commun 8. https://doi.org/10.1186/s40478-020-00967-w

Xiao, Q., Xu, X., Tu, J., 2020. Chronic optogenetic manipulation of basolateral amygdala astrocytes rescues stress-induced anxiety. Biochem Biophys Res Commun 533, 657–664. https://doi.org/10.1016/J.BBRC.2020.09.106

Yanai, S., Endo, S., 2021. Functional Aging in Male C57BL/6J Mice Across the Life-Span: A Systematic Behavioral Analysis of Motor, Emotional, and Memory Function to Define an Aging Phenotype. Front Aging Neurosci 13, 457. https://doi.org/10.3389/FNAGI.2021.697621/BIBTEX

York, E.M., Ledue, J.M., Bernier, L.P., Macvicar, B.A., 2018. 3DMorph Automatic Analysis of Microglial Morphology in Three Dimensions from Ex Vivo and In Vivo Imaging. eNeuro 5. https://doi.org/10.1523/ENEURO.0266-18.2018

Zhou, Y., Zhu, H., Liu, Z., Chen, X., Su, X.J., Ma, C., Tian, Z., Huang, B., Yan, E., Liu, X., Ma, L., 2019. A ventral CA1 to nucleus accumbens core engram circuit mediates conditioned place preference for cocaine. Nature Neuroscience 2019 22:12 22, 1986–1999. https://doi.org/10.1038/s41593-019-0524-y